Title

Low CD38 Identifies Progenitor-like Inflammation-Associated Luminal Cells that Can Initiate Human Prostate Cancer and Predict Poor Outcome

Journal

Cell Reports, 17(10)

ISSN

2639-1856

Authors

Liu, Xian

Grogan, Tristan R

Hieronymus, Haley

et al.

Publication Date

2016-12-01

DOI

10.1016/j.celrep.2016.11.010

Peer reviewed

Article

Cell Reports

Low CD38 Identifies Progenitor-like Inflammation-Associated Luminal Cells that Can Initiate Human Prostate Cancer and Predict Poor Outcome

Graphical Abstract

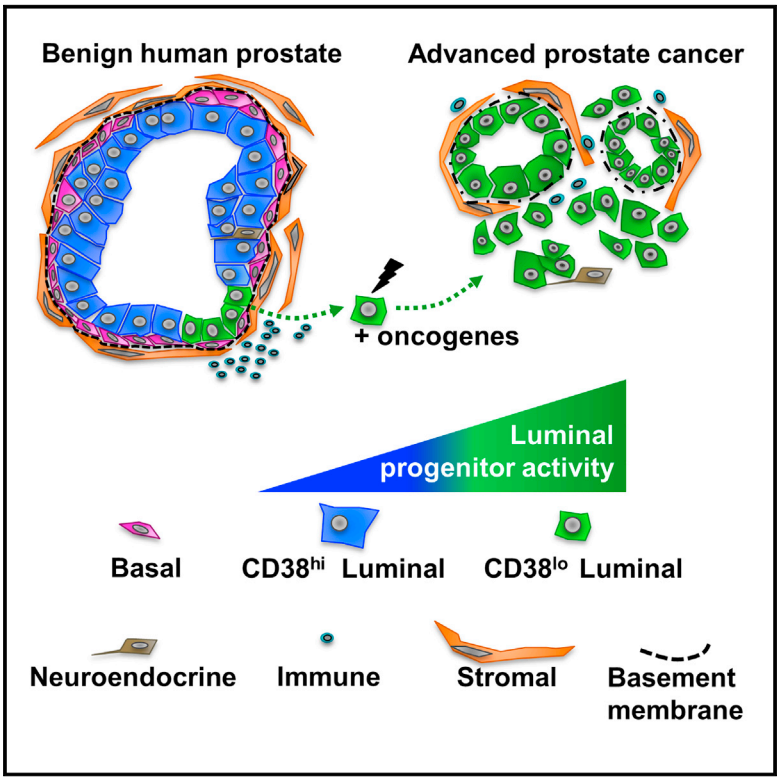

Authors

Xian Liu, Tristan R. Grogan, Haley Hieronymus, ..., Jiaoti Huang, Owen N. Witte, Andrew S. Goldstein

Correspondence

agoldstein@mednet.ucla.edu

In Brief

Chronic inflammation of the prostate is a risk factor for cancer, but how inflammation increases disease risk remains poorly defined. Liu et al. show that luminal progenitor cells expressing low levels of CD38 are expanded around inflammation, and these progenitors are target cells that can initiate human prostate cancer.

Highlights

- Low expression of CD38 enriches for luminal progenitor cells in human prostate
- CD38^{lo} luminal cells are localized in proximity to prostatic inflammation
- CD38^{lo} luminal cells are target cells for aggressive human prostate cancer
- Low CD38 in prostate cancer is prognostic for biochemical recurrence and metastasis

Accession Numbers

GSE89050

Liu et al., 2016, Cell Reports *17*, 2596–2606
December 6, 2016
http://dx.doi.org/10.1016/j.celrep.2016.11.010

CellPress

OPEN ACCESS
CellPress

Cell Reports
Article

Low CD38 Identifies Progenitor-like Inflammation-Associated Luminal Cells that Can Initiate Human Prostate Cancer and Predict Poor Outcome

Xian Liu,[1] Tristan R. Grogan,[3] Haley Hieronymus,[4] Takao Hashimoto,[1] Jack Mottahedeh,[1] Donghui Cheng,[5] Lijun Zhang,[2] Kevin Huang,[2] Tanya Stoyanova,[6,15] Jung Wook Park,[6] Ruzanna O. Shkhyan,[1] Behdokht Nowroozizadeh,[7] Matthew B. Rettig,[8,9,10,11] Charles L. Sawyers,[4] David Elashoff,[3,11] Steve Horvath,[12,13] Jiaoti Huang,[5,7,11,16] Owen N. Witte,[2,5,6,11,14] and Andrew S. Goldstein[1,5,10,11,17,*]

[1]Molecular, Cell and Developmental Biology, University of California, Los Angeles, Los Angeles, CA 90095, USA
[2]Molecular and Medical Pharmacology, David Geffen School of Medicine, University of California, Los Angeles, Los Angeles, CA 90095, USA
[3]Department of Medicine Statistics Core, David Geffen School of Medicine, University of California, Los Angeles, Los Angeles, CA 90095, USA
[4]Programs in Human Oncology and Pathogenesis, Memorial Sloan Kettering Cancer Center, New York, NY 10065, USA
[5]Eli and Edythe Broad Center of Regenerative Medicine and Stem Cell Research, University of California, Los Angeles, Los Angeles, CA 90095, USA
[6]Microbiology, Immunology and Molecular Genetics, University of California, Los Angeles, Los Angeles, CA 90095, USA
[7]Pathology and Laboratory Medicine, David Geffen School of Medicine, University of California, Los Angeles, Los Angeles, CA 90095, USA
[8]Division of Hematology-Oncology, David Geffen School of Medicine, University of California, Los Angeles, Los Angeles, CA 90095, USA
[9]VA Greater Los Angeles Healthcare System, Los Angeles, CA 90024, USA
[10]Urology, David Geffen School of Medicine, University of California, Los Angeles, Los Angeles, CA 90095, USA
[11]Jonsson Comprehensive Cancer Center, University of California, Los Angeles, Los Angeles, CA 90095, USA
[12]Human Genetics, David Geffen School of Medicine, University of California, Los Angeles, Los Angeles, CA 90095, USA
[13]Biostatistics, UCLA Fielding School of Public Health, University of California, Los Angeles, Los Angeles, CA 90095, USA
[14]Howard Hughes Medical Institute, University of California, Los Angeles, Los Angeles, CA 90095, USA
[15]Present address: Department of Radiology, Canary Center at Stanford for Cancer Early Detection, Stanford University School of Medicine, Palo Alto, CA 94304, USA
[16]Present address: Department of Pathology, Duke University School of Medicine, Durham, NC 27710, USA
[17]Lead Contact
*Correspondence: agoldstein@mednet.ucla.edu
http://dx.doi.org/10.1016/j.celrep.2016.11.010

SUMMARY

Inflammation is a risk factor for prostate cancer, but the mechanisms by which inflammation increases that risk are poorly understood. Here, we demonstrate that low expression of CD38 identifies a progenitor-like subset of luminal cells in the human prostate. CD38^{lo} luminal cells are enriched in glands adjacent to inflammatory cells and exhibit epithelial nuclear factor κB (NF-κB) signaling. In response to oncogenic transformation, CD38^{lo} luminal cells can initiate human prostate cancer in an in vivo tissue-regeneration assay. Finally, the CD38^{lo} luminal phenotype and gene signature are associated with disease progression and poor outcome in prostate cancer. Our results suggest that prostate inflammation expands the pool of progenitor-like target cells susceptible to tumorigenesis.

INTRODUCTION

An inflammatory microenvironment is a critical component driving tumorigenesis, from cancer initiation to metastasis to end-stage treatment-resistant lethal disease (Das Roy et al., 2009; Gurel et al., 2014; Liu et al., 2013; Wang et al., 2015). In many adult tissues, cancers originate in sites of chronic inflammation (Coussens and Werb, 2002). It is hypothesized that sustained proliferative signals from inflammatory cells can cooperate with oncogenic events to promote tumorigenesis (De Marzo et al., 2007). Mouse models have been developed that recapitulate features of inflammation in the tumor microenvironment and demonstrate a role for defined immune cell types and inflammatory cytokines in cancer initiation and progression (Ammirante et al., 2010; Garcia et al., 2014). Few studies have investigated the functional consequences of inflammation in human epithelial tissues.

Chronic inflammation of the prostate is a risk factor for aggressive prostate cancer (Gurel et al., 2014; Sfanos and De Marzo, 2012; Shafique et al., 2012), as men with chronic inflammation in benign tissues have greater than double the risk for developing high-grade disease compared to men with no inflammation in their benign biopsy cores (Gurel et al., 2014). Groundbreaking work from De Marzo and colleagues has defined a series of histological changes associated with chronic inflammation in the human prostate known as proliferative inflammatory atrophy (PIA) as a likely precursor for prostate cancer (De Marzo et al., 1999, 2007). In PIA, the luminal epithelial layer in close proximity to infiltrating immune cells is

described as having an atrophic appearance with an increased proliferative index, suggesting a regenerative response (De Marzo et al., 2003). Luminal cells associated with PIA exhibit reduced androgen signaling and increased expression of the anti-apoptotic factor BCL2 (De Marzo et al., 1999, 2003). PIA cells are thought to exhibit an intermediate state of differentiation between basal and luminal cells and are predicted to serve as target cells in prostate tumorigenesis (van Leenders et al., 2003). Several groups have modeled inflammation in the mouse prostate using a variety of approaches, including bacterial infection (Elkahwaji et al., 2009; Khalili et al., 2010; Kwon et al., 2014), high-fat diet (Kwon et al., 2016), and adoptive transfer of prostate-targeting T cells (Haverkamp et al., 2011), demonstrating that prostatic inflammation is associated with increased epithelial proliferation. However, mouse models may not recapitulate the complex environment of aged human prostate tissues exposed to chronic inflammation for years prior to the development of prostate cancer (Gurel et al., 2014).

Lineage tracing in the mouse has demonstrated that both basal and luminal cells are sufficient to initiate prostate cancer following *Pten* deletion, with differences in tumor outcome depending on the genetic background and status of *Nkx3-1* (Choi et al., 2012; Lu et al., 2013; Wang et al., 2013). Luminal cells can initiate murine prostate cancer in diverse genetically engineered mouse models (Wang et al., 2014), while purified basal cells can respond to a range of oncogene combinations to generate murine tumors using a tissue-regeneration approach (Lawson et al., 2010). In the human prostate, we and others have demonstrated that basal cells isolated from benign human prostate can give rise to tumors following oncogenic transformation (Goldstein et al., 2010; Stoyanova et al., 2013; Taylor et al., 2012). To date, luminal cells in the human prostate have only been shown to initiate indolent-like tumors with limited proliferation (Park et al., 2016), perhaps due to the low rate of proliferation among luminal cells (De Marzo et al., 1999). In contrast, luminal cell proliferation is increased in regions associated with inflammation in human prostate (De Marzo et al., 1999), suggesting that luminal cells isolated from regions with inflammation may exhibit progenitor cell features and give rise to aggressive prostate cancer.

Here, we report that expression of the luminal cell marker CD38 is heterogeneous in the human prostate. We used low expression of CD38 to isolate a subset of p63-negative, keratin 14 (K14)-negative, keratin 18 (K18)-positive luminal cells from primary benign human prostate with unique functional and molecular properties compared to $CD38^{hi}$ luminal cells. Human prostate $CD38^{lo}$ $CD38^{lo}$ luminal cells are expanded in regions with inflammation, express markers of PIA, and are enriched for progenitor activity. In human tissues, CD38 is inversely correlated with prostate cancer progression and low CD38 mRNA in tumors is prognostic for biochemical recurrence and metastasis. Finally, $CD38^{lo}$ luminal cells can initiate prostate cancer in response to oncogenic transformation using a human tissue regeneration model in immune-deficient mice. These collective results support inflammation-associated luminal cells as a target cell for aggressive prostate cancer.

RESULTS

Differential Expression of CD38 Enables Isolation of Two Distinct Luminal Subsets

CD38 is reported as a marker of luminal cells in the human prostate (Kramer et al., 1995), and gene expression studies demonstrate that CD38 mRNA can distinguish basal from luminal cells (Smith et al., 2015). We measured cell-surface expression of CD38 by flow cytometry and confirmed that within the $EpCAM^+$ $CD45^-$ epithelial fraction, CD38 is expressed by $CD26^+$ luminal cells, but not by CD49f-hi basal cells (Figure 1A). Upon performing immunohistochemical staining for CD38 in human prostate tissue, we noted heterogeneous staining within the luminal layer, including areas where CD38 expression was reduced within individual glands (Figure 1B).

We set out to viably isolate luminal cells based on variations in surface expression of CD38 using fluorescence-activated cell sorting (FACS). After removing $CD45^+$ immune cells and gating on $EpCAM^+$ epithelial cells, we observed three cell populations based on expression of CD49f and CD38 (Figure 1C) in preparations of dissociated cells isolated from benign human prostate tissue. Intracellular flow cytometry revealed that both CD49f-lo $CD38^{hi}$ and $CD49f^{lo}$ $CD38^{lo}$ subsets expressed high levels of the luminal marker K18 (Figures 1D and S1A). Western blot analysis demonstrated that basal markers p63 and K14 are not expressed in either luminal subset (Figure 1E). We noted elevated expression of keratin 5 (K5), a marker of a proposed intermediate-type luminal cell (van Leenders et al., 2003), in $CD38^{lo}$ compared to $CD38^{hi}$ luminal cells (Figure S1B). Following cell isolation, cell diameters were measured to examine differences in size among the three epithelial populations. $CD38^{lo}$ luminal cells demonstrated an average diameter intermediate between basal and $CD38^{hi}$ luminal cells (Figure 1F). These findings indicate that CD38 stratifies luminal cells into two distinct subpopulations. Importantly, $CD38^{lo}$ luminal cells do not express CD26 by flow cytometry (Figure S1C). These data indicate that $CD38^{lo}$ luminal cells are distinct from $CD26^+$ luminal cells and represent a population not previously investigated in prior studies (Karthaus et al., 2014; Park et al., 2016; Stoyanova et al., 2013).

$CD38^{lo}$ Luminal Cells Are Enriched for Progenitor Activity Compared to $CD38^{hi}$ Luminal Cells

In order to test the functional capacity of distinct luminal subsets, it is important to remove any potential contaminating basal cells that are highly clonogenic in progenitor assays (Goldstein et al., 2008; Karthaus et al., 2014; Park et al., 2016). We used a double-sorting approach to isolate highly purified preparations of $CD38^{lo}$ and $CD38^{hi}$ luminal cells from benign human prostate tissue and confirmed an absence of basal cells based on lack of expression of CD49f (Figure 2A) and p63 (Figures S2A and S2B). In a two-dimensional colony-forming assay and a three-dimensional sphere-forming assay (Lawson et al., 2010; Lukacs et al., 2010), $CD38^{lo}$ luminal cells exhibited progenitor activity intermediate between the highly clonogenic basal cells and the $CD38^{hi}$ luminal cells (Figures 2B and 2C). In a culture system adapted for the growth of human prostate-like tissue in vitro (Karthaus et al., 2014), $CD38^{lo}$ luminal cells were highly (4- to 5-fold) enriched for organoid formation compared to $CD38^{hi}$ luminal cells

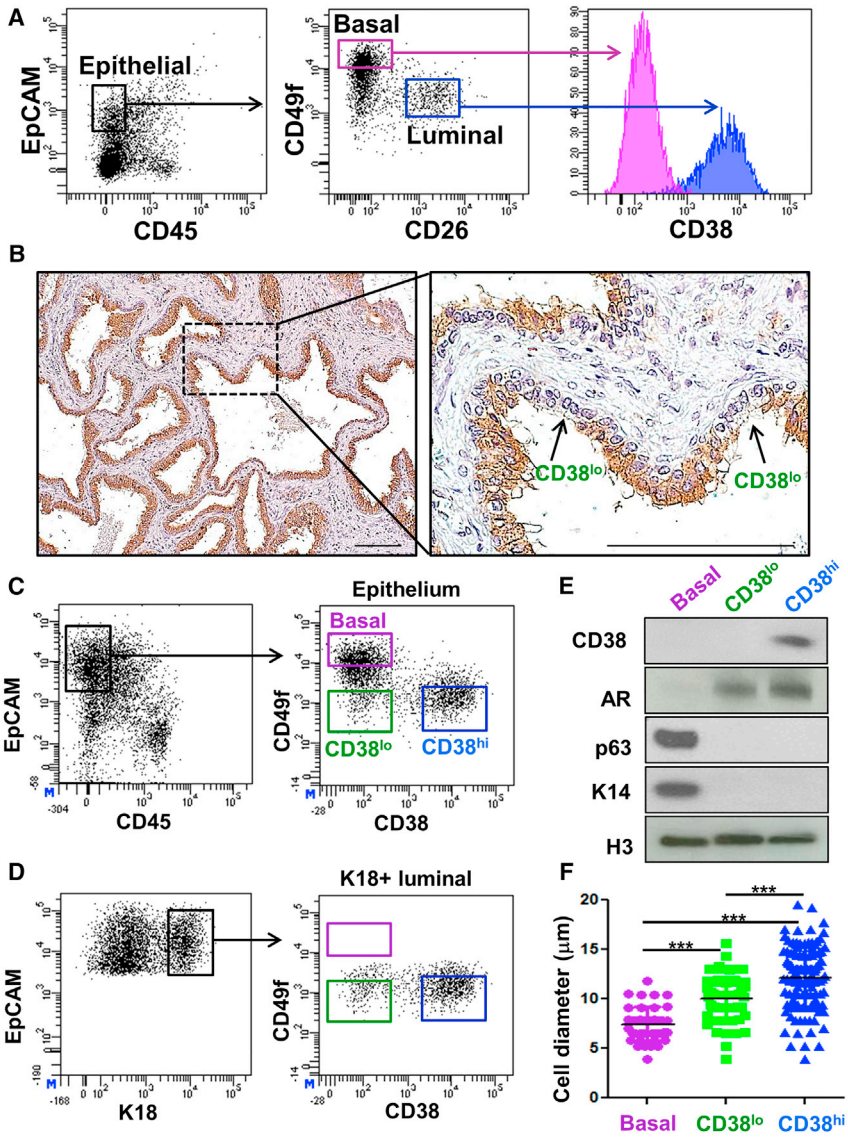

Figure 1. Differential Expression of CD38 Enables Isolation of Discrete Luminal Subsets from Fresh Human Prostate Tissue

(A) Fluorescence-activated cell sorting analysis of dissociated benign human prostate cells demonstrates CD38 expression in EpCAM$^+$ CD45$^-$ CD26$^+$ luminal cells, but not in EpCAM$^+$ CD45$^-$ CD49f-hi basal cells.

(B) Immunohistochemical analysis of benign human prostate glands stained with anti-CD38 antibodies. Boxed region is magnified in the right. Arrows identify rare CD38^{lo} cells lining the gland. Scale bars, 50 μm.

(C) Fluorescence-activated cell sorting analysis of dissociated benign human prostate cells gated on EpCAM$^+$ CD45$^-$ cells and further stained with antibodies against CD49f and CD38.

(D) Intracellular flow cytometry for Keratin 18 (K18) and surface staining for CD38 and CD49f. Gating on K18$^+$ luminal cells demonstrates two luminal populations in right plot.

(E) Western blot analysis of three epithelial subsets from representative patient sample stained with antibodies against CD38, AR, p63, keratin 14 (K14), and histone H3 as a loading control.

(F) Sorted cells were counted in a hemocytometer, and average cell diameter (in microns) was quantified for each population from multiple patient samples.

Data represent mean ± SEM with replicate points shown. Newman-Keuls multiple comparison test with ***$p < 0.0001$.

(Figure 2D). CD38^{lo} luminal cell-derived organoids contained cells expressing both basal (K5 and p63) and luminal (K8) markers (Figures 2E and S2C), similar to what has been reported for CD26$^+$ luminal cells (Karthaus et al., 2014). When double-sorted cells were plated at single-cell density and visually confirmed, 5% (9/177) of single CD38^{lo} luminal cells were capable of generating organoids (Figure 2F), which is considerably greater than the rate of CD38^{hi} luminal cells (1/142) and the 1% rate reported for CD26$^+$ luminal cells (Karthaus et al., 2014; Park et al., 2016).

CD38^{lo} Luminal Cells Exhibit an Inflammatory Signature

To investigate potential mechanisms regulating differential progenitor activity, we performed RNA sequencing (RNA-seq) and microarray analysis. We generated an RNA-seq signature comprised of 449 genes greater than 2 fold-enriched in CD38^{lo} luminal cells compared to CD38^{hi} luminal cells and greater than 1.5-fold enriched compared to basal cells (Table S1). We found that CD38^{lo} luminal cells express elevated levels of BCL2, a gene previously associated with PIA (De Marzo et al., 1999) (Figure 3A). A number of inflammatory-related genes including cytokines (*Tnf*, *Il6*, and *Il8*) and chemokines (*Cxcl1*, *Cxcl2*, *Cxcl3*, *Cxcl6*, *Ccl2*, and *Ccl20*) are enriched in CD38^{lo} luminal cells (Figure 3A). We performed pathway analysis using DAVID Bioinformatics (Huang da et al., 2009) and found the most significant keywords included "inflammatory signaling" and "immune response" (Figure 3B). The significant pathways and inflammatory-related genes were confirmed to be upregulated in CD38^{lo} luminal cells by microarray analysis. We confirmed activation of the nuclear factor κB (NF-κB) pathway at the protein level based on phosphorylated p65 and expression of BCL2 by western blot (Figure 3C). In tissue sections, we found that phosphorylated p65 was highly expressed in CD38^{lo} luminal cells in a pattern inversely correlated with CD38 (Figure 3D). Ingenuity pathway analysis identified tumor necrosis factor alpha (TNF) as a likely upstream regulator of CD38^{lo} luminal cells. We confirmed that TNF is expressed in CD38^{lo} cells but absent from CD38^{hi} luminal cells by immunohistochemistry (Figure S3A), suggesting that TNF may activate NFkB signaling in CD38^{lo} cells. We observed a diminution of p65 phosphorylation and reduced expression of BCL2 in

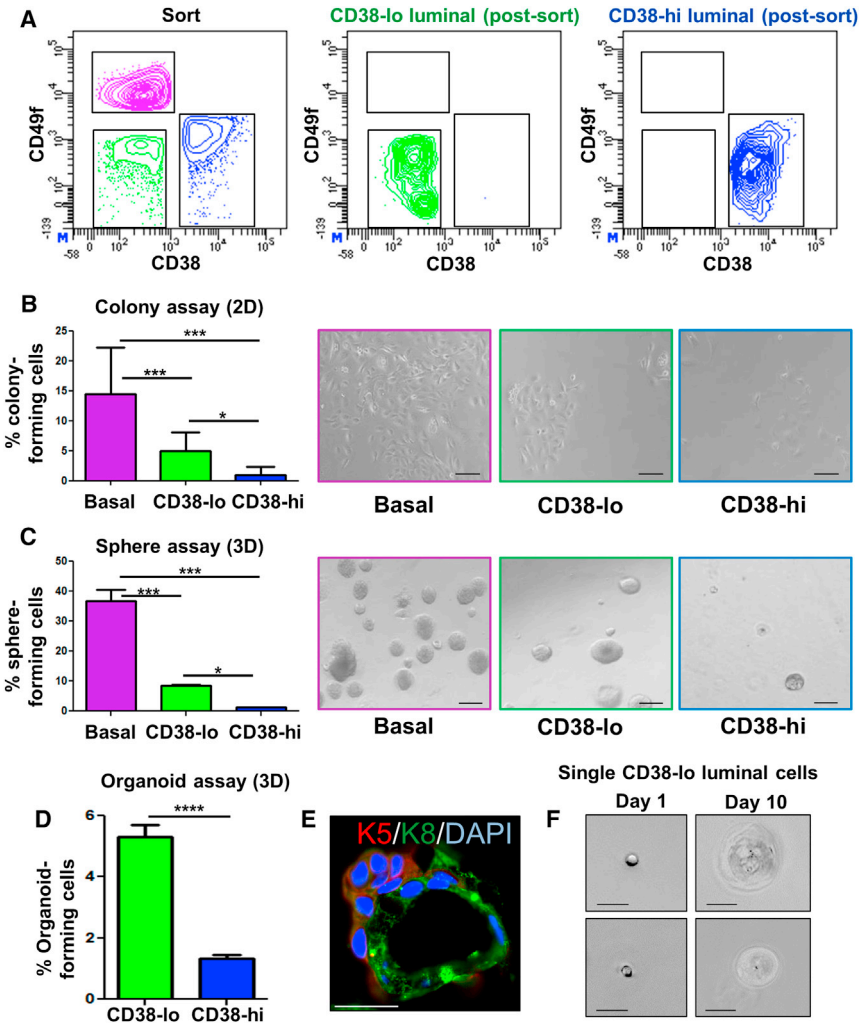

Figure 2. CD38^{lo} Cells Exhibit Greater Progenitor Activity than CD38^{hi} Luminal Cells In Vitro

(A) Flow cytometry analysis for CD49f and CD38 dissociated human prostate epithelium as gated during the sort (left), and post-sort analysis of CD38^{lo} and CD38^{hi} luminal cells prior to in vitro culture.

(B and C) Primary human benign prostate epithelial cells (EpCAM^{+} CD45^{-}) were sorted into basal cells, CD38^{lo} and CD38^{hi} luminal subsets and plated for in vitro colony and sphere forming assays. Results from in vitro two-dimensional colony-forming assay (B) and three-dimensional sphere-forming assay (C) measured 10–14 days after plating benign human prostate epithelial subsets. Data represent pooled experiments from three independent patients. Mean ± SEM is shown. Statistics represent Newman-Keuls multiple comparison test with *$p < 0.05$, ***$p < 0.0005$. Representative images of outgrowths from each epithelial subset are taken at 10–14 days. Scale bars, 250 μm.

(D) CD38^{lo} luminal cells generate significantly more organoids than CD38^{hi} luminal cells, four replicates per sample, representative of five independent patient samples. Statistics represent Two-tailed unpaired t test with ****$p < 0.0001$.

(E) Representative staining of CD38^{lo} luminal cell-derived organoids for K5, K8, and DAPI nuclear counterstain. Scale bars, 50 μm.

(F) Representative images of organoids forming from single CD38^{lo} luminal cells taken at day 1 and day 10. Scale bars, 100 μm.

CD38^{lo} cells following treatment with the NF-κB pathway inhibitor ACHP (Figure S3B). In a functional assay, ACHP treatment blocked the organoid-forming progenitor activity of CD38^{lo} luminal cells to a greater extent than other epithelial subsets (Figure S3C).

CD38^{lo} Luminal Cells Are Expanded in Glands Adjacent to Inflammation

Based on their gene expression profiling, including genes associated with PIA and inflammation, we investigated expression of CD38 in regions containing inflammatory infiltration (Figure 3E). Staining for CD38 and CD45 on serial slides indicates that CD38 expression is reduced adjacent to CD45^{+} cells (Figure 3F). We stained for a panel of immune cell subsets and found evidence of CD4^{+} and CD8^{+} T cells, CD11c^{+} and CD68^{+} myeloid cells, and CD20^{+} B cells adjacent to regions of the gland with low expression of CD38 (Figure S3D). In order to better define the relationship between CD38 expression and inflammation, we stratified glands into three categories: normal, inflamed, and atrophic, as classified by an expert pathologist. Inflamed glands were identified by pathologic criteria and confirmed with CD45 staining. Atrophic glands were identified by pathologic criteria and generally measured less than 20 μm from the basement membrane to the lumen in contrast to normal glands (Figure S3E). Loss of CD38 expression was measured in 95% (38/40) of inflamed glands, 88% (35/40) of atrophic glands, and only 10% (4/40) of normal glands from representative patient samples. Similar results were obtained for TNF, with strong expression in inflamed (38/40) and atrophic glands (33/40) with rare expression in normal glands (1/40). We further explored the connection between immune cells and CD38^{lo} luminal cells by flow cytometry in benign human prostate tissues from 29 distinct patient samples. We found a statistically significant association between the percentage of CD45^{+} immune cells and the proportion of luminal cells exhibiting a CD38^{lo} surface phenotype (Figures 3G and S3F).

Reduced Androgen Signaling in CD38^{lo} Luminal Cells

CD38^{lo} luminal cells express lower levels of *Klk3*, the gene for prostate-specific antigen (PSA) and other androgen-target genes (*Klk2*, *Klk4*, *Msmb*, *Acpp*, and *Fkbp5*) (Figure 3A), consistent with reduced androgen signaling observed in PIA lesions (De Marzo et al., 1999). Similar results were observed by microarray analysis. qPCR confirmed differences in *Klk3* mRNA between the luminal subsets (Figure 4A). In contrast, levels of the luminal gene K8 were not significantly different (Figure 4A). Using

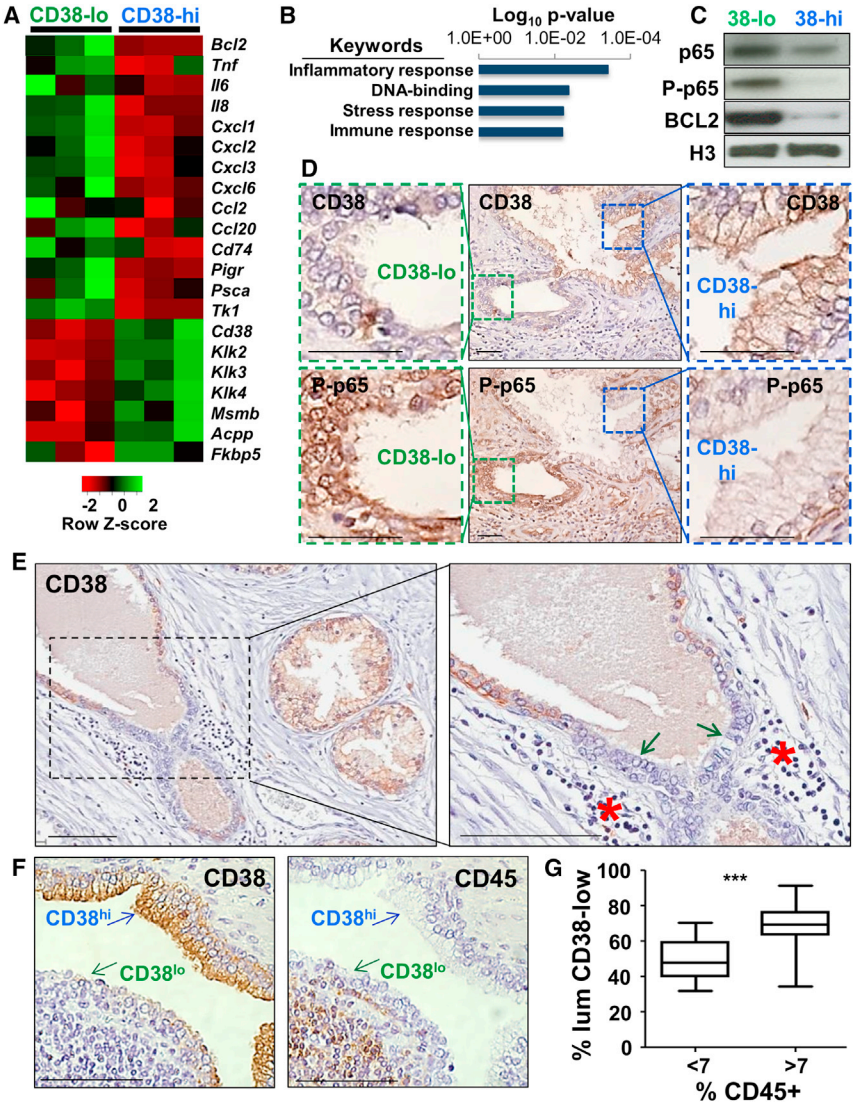

Figure 3. CD38^{lo} Luminal Cells Are Associated with Inflammation

(A) Heatmap of RNA-sequencing results of CD38^{lo} luminal cells and CD38^{hi} luminal cells from three independent patients.

(B) DAVID bioinformatics analysis (SP_PIR_KEYWORDS) of the CD38^{lo} luminal gene signature with log(10) p values plotted.

(C) Western blot analysis of CD38^{lo} and CD38^{hi} luminal cells from a representative benign human prostate sample stained for total p65, phosphorylated p65 (P-p65 S536), BCL2, and histone H3 as a loading control.

(D) Immunohistochemical analysis of benign human prostate stained for CD38 and phosphorylated p65 (S536) on serial sections indicating an inverse relationship between expression of CD38 and P-p65. Scale bars, 50 μm.

(E) Immunohistochemical analysis of benign human prostate glands stained with anti-CD38 antibodies. Boxed regions are magnified in the bottom row. Arrows denote regions of epithelium with low expression of CD38 in close proximity to red asterisk identifying areas with immune cell infiltration. Scale bars, 100 μm.

(F) Immunohistochemistry on serial slides stained for CD38 and CD45. Scale bars, 100 μm.

(G) Increased proportion of luminal cells with CD38^{lo} phenotype from 29 samples plotted as CD45^{+} cells less than or greater than 7% of total prostate. Statistics represent two-tailed t test; ***p = 0.0003.

immunohistochemistry, we confirmed diminished expression of androgen targets PSA, FKBP5, and MSMB in CD38^{lo} luminal cells at the protein level (Figure 4B). Androgen receptor (AR) target NKX3-1 was also reduced in CD38^{lo} luminal cells (Figure S4). We hypothesized that low androgen signaling in CD38^{lo} luminal cells may be due to low levels of AR. While AR is expressed in CD38^{lo} cells, protein levels are reduced compared to CD38^{hi} luminal cells (Figures 1E and 4C).

CD38^{lo} Luminal Phenotype Is Associated with Disease Progression and Poor Outcome

CD38 expression was previously reported to be reduced in a small cohort of prostate cancer specimens compared to benign prostate tissues (Kramer et al., 1995). We examined expression of CD38 in a tissue microarray containing tissue cores from 267 patients with prostate cancer (Gollapudi et al., 2013) (Table S2) and found the highest protein expression of CD38 in benign glands, with reduced expression in PIN and prostate cancer (Figures 5A and 5B; Table S3). The lowest expression of CD38 was found in the most advanced tumors based on Gleason grade (Figures 5A and 5B). Immunohistochemical staining was verified using two different anti-CD38 antibodies (Figure S5). While the average CD38 expression level was statistically significantly associated with time to biochemical recurrence, CD38 expression in cancer specimens was not statistically significant (Table S4).

Using the Memorial Sloan Kettering Cancer Center (MSKCC) dataset (Hieronymus et al., 2014; Taylor et al., 2010), we found that low CD38 mRNA in prostatectomy-derived prostate cancer samples is prognostic for biochemical recurrence and metastasis (Figures 5C and 5D) in a statistically significant manner (Table S5). Importantly, low CD38 mRNA status is statistically significantly associated with both biochemical recurrence and metastasis after correction for Stephenson nomogram score (Stephenson et al., 2005), which includes both clinical and pathological variables (Table S5). Low CD38 mRNA is also prognostic for biochemical recurrence in the Cancer Genome Atlas (TCGA) dataset (Network, 2015) (Figure 5E). Upon stratifying tumors based on genotype, we found that low CD38 mRNA expression was associated with SPINK1 outlier status, but not ETS-related gene (ERG) rearrangements, in the MSKCC cohort (Figure S6A).

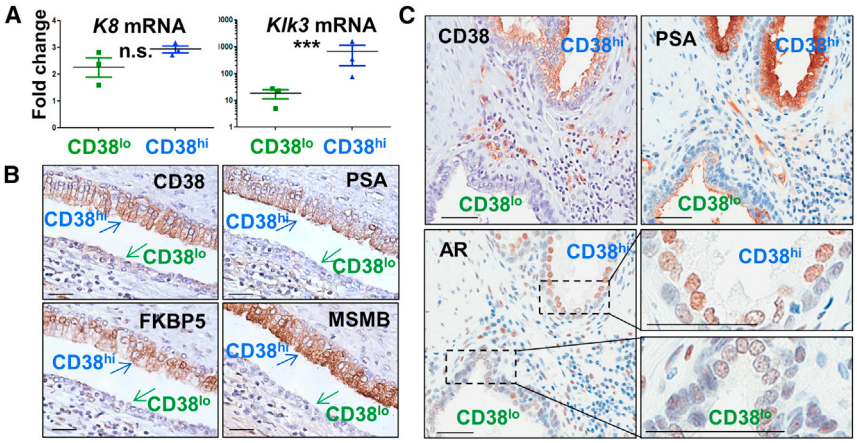

Figure 4. CD38^{lo} Luminal Cells Exhibit Reduced Androgen Signaling

(A) Relative expression of *Klk3* or *K8* compared to *Gapdh* in basal cells as measured by qPCR of basal, CD38^{lo}, and CD38^{hi} luminal cells isolated from three independent patient samples. Data are presented as mean ± SEM with replicate points shown. *Klk3* is shown on a log scale. Two-tailed unpaired t test between CD38^{lo} and CD38^{hi} luminal subsets; ***p = 0.0004.

(B) Immunohistochemical analysis of benign human prostate stained for CD38 and AR targets PSA, FKBP5, and MSMB. Scale bars, 100 μm.

(C) Immunohistochemistry for CD38, PSA, and AR distinguishes CD38^{hi} and CD38^{lo} regions. AR expression is magnified to demonstrate reduced expression in CD38^{lo} cells. Scale bars, 50 μm.

To determine whether the CD38^{lo} luminal gene signature could provide value in predicting patient survival, we turned to a Swedish watchful waiting cohort containing outcome data for 281 men (Sboner et al., 2010). The mean of the scaled expression values of the CD38^{lo} luminal genes was significantly (p = 0.037) associated with all-cause mortality after adjusting for Gleason sum, age, and cancer percentage (Table S6A). When we analyzed the patients most at risk for prostate cancer-related mortality, with a Gleason score greater than or equal to 7 and follow-up within 5 years, we found a statistically significant difference (p = 0.007) between patients whose expression values lie in the top third (CD38^{lo} luminal-like) versus all others (Figure S6B; Table S6C). The statistical significance of the CD38^{lo} signature within this restricted group reached p = 0.0007 after adjusting for Gleason sum, age, and cancer percentage (Table S6B). The CD38^{lo} luminal gene signature is inversely correlated with the AR signature score (Hieronymus et al., 2006) in prostate tumor specimens in a statistically significant manner in multiple cohorts (Figure S6C). We confirmed that the effect of the CD38^{lo} signature was independent of the AR signature (Hieronymus et al., 2006; Nelson et al., 2002) and a previously reported immune signature (Jin et al., 2014) (Tables S6D and S6E).

CD38^{lo} Luminal Cells Express the Therapeutic Target PSCA

While CD38 expression is low in the most aggressive tumors, we reasoned that genes in the CD38^{lo} luminal cell signature may be expressed in advanced disease and might serve as positive markers of this cell population. We used immunohistochemistry to investigate expression of prostate stem cell antigen (PSCA), a therapeutic target expressed in aggressive, metastatic, and castration-resistant prostate cancer (Gu et al., 2000). *Psca* is enriched in CD38^{lo} cells (Figure 3A) but has not been previously associated with PIA. In tissue sections, PSCA expression was observed more commonly in inflamed (28/40) glands than atrophic (15/40) or benign (12/40) glands, in an expression pattern inversely correlated with CD38 (Figure 6A). In some regions, these two markers can distinguish benign glands (CD38^{hi} PSCA-low) from cancer (CD38^{lo} PSCA-hi) (Figure 6B). We hypothesized that CD38^{lo} PSCA-hi cancers may arise from the transformation of CD38^{lo} PSCA-hi luminal cells.

CD38^{lo} Luminal Cells Can Regenerate Glands and Initiate Human Prostate Cancer

To determine the functional capacity of CD38^{lo} luminal cells in tissue-regeneration and disease-initiation, we turned to an in vivo regeneration assay where human prostate epithelial cells are combined with urogenital sinus mesenchyme cells (UGSM) in Matrigel and transplanted subcutaneously into immune-deficient mice (Goldstein et al., 2010, 2011). To track human epithelial cells, we introduced genes for red and green fluorescent proteins into CD38^{lo} luminal cells prior to in vivo transplantation (Figures 7A and S7A). Due to low cell numbers insufficient for direct in vivo implantation, we utilized a recently published approach to expand isolated cells in organoid culture for 1–2 weeks prior to transplantation (Park et al., 2016). An average of 200 lentiviral-transduced organoids derived from CD38^{lo} luminal cells were combined with UGSM and implanted into NOD-SCID-IL2Rγ^{null} mice. 8 weeks post-transplantation, we identified prostatic glands containing both luminal cells expressing K8 and AR and basal cells expressing K5 and p63 (Figure 7B). Lentiviral transduced human epithelial structures in regenerated tissues could be identified based on fluorescent signal, whereas control grafts without human cells lacked any epithelial structures or fluorescence (Figure S7C).

Oncogenes previously shown to transform primary human prostate (Goldstein et al., 2010; Stoyanova et al., 2013) (Myc, myristoylated AKT, and AR) were introduced into double-sorted CD38^{lo} luminal cells via lentiviral delivery prior to in vitro expansion and in vivo transplantation. We identified features of human prostate adenocarcinoma, including expression of the luminal markers K8, PSA, and AR and an absence of the basal markers K5 and p63 in regenerated tumors derived from oncogene-expressing CD38^{lo} luminal cells (Figure 7C). Regenerated tumors exhibited expression of oncogenes (Figure S7B). Importantly, tumors exhibited the PSCA-hi CD38^{lo} luminal phenotype and a high frequency of cells expressed the proliferative marker Ki67 (>40% Ki67^{+}) (Figure 7C). Results were confirmed using tissue from four independent patient samples. These findings indicate

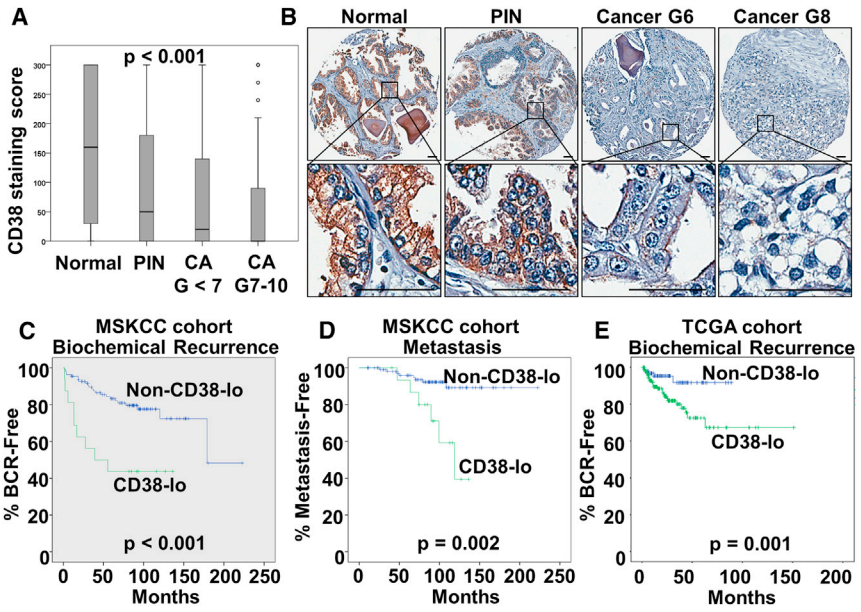

Figure 5. Association of CD38^{lo} Phenotype with Prostate Cancer Progression

(A) Plot of composite CD38 staining score in tissues histologically classified as normal, prostate intraepithelial neoplasia (PIN), or prostate cancer (CA) with Gleason scores less than 7 or 7–10. Middle bar represents mean value. The overall effect of different levels of CD38 among the prostate regions was confirmed ($p < 0.001$).

(B) Representative immunohistochemical images of normal, PIN, Gleason 6, and Gleason 8 cancer stained for CD38, with high-power images below. Scale bars, 50 μm.

(C and D) Survival analysis from MSKCC cohort measuring biochemical recurrence (C) and metastasis (D) for tumors containing CD38 mRNA 1 SD below the mean compared to the remainder (non-CD38^{lo}). Log rank (Mantel Cox) $p < 0.001$ (recurrence in C) and $p = 0.002$ (metastasis in D).

(E) Survival analysis from the TCGA cohort measuring biochemical recurrence comparing CD38 expression less than (CD38^{lo}) or greater than (non- CD38^{lo}) the mean *Z* score. Log rank (Mantel Cox) $p = 0.001$.

that CD38^{lo} luminal cells can initiate human prostate cancer in vivo.

DISCUSSION

Chronic inflammation is associated with cancer initiation, progression, metastasis, and treatment resistance in a range of tumor types including prostate cancer (Das Roy et al., 2009; Gurel et al., 2014; Liu et al., 2013; Wang et al., 2015). In mouse models, several groups have established a tumor-promoting functional contribution of distinct immune cell types to prostate cancer, including B cells and myeloid-derived suppressor cells (Ammirante et al., 2010; Garcia et al., 2014). However, little is known about the influence of inflammation on the function of human prostate epithelium prior to tumor formation. De Marzo and colleagues have proposed that inflammation may be an inciting event in prostate transformation and that PIA cells may serve as target cells for tumor initiation (De Marzo et al., 1999, 2003, 2007). Our results demonstrate that PIA-like CD38^{lo} luminal cells can initiate human prostate cancer.

Several groups have isolated human prostate luminal cells based on low expression of CD49f or high expression of CD26 for functional studies (Goldstein et al., 2010; Karthaus et al., 2014; Park et al., 2016; Stoyanova et al., 2013). We found that CD26 and CD38 identify an analogous population of prostate luminal cells (Figure S1C). While rare cells within the CD26^{+} or CD38^{hi} luminal cell population exhibit organoid-forming activity, ~99% of cells in this subset do not exhibit progenitor features (Figures 2B–2D; Karthaus et al., 2014; Park et al., 2016). In contrast, CD38^{lo} luminal cells are enriched for progenitor activity in 2D and 3D progenitor assays, as 5% of CD38^{lo} luminal cells are capable of generating organoids (Figure 2D), similar to the rate of *Lgr5*-GFP-hi intestinal stem cells (Sato et al., 2009). Therefore, identifying the signaling pathways active in CD38^{lo} luminal cells may yield mechanisms regulating luminal progenitor activity.

We found that CD38^{lo} and CD38^{hi} luminal cells have distinct transcriptional signatures. While androgen signaling is active in CD38^{hi} luminal cells (Figure 4), CD38^{lo} luminal cells exhibit elevated NF-κB signaling (Figure 3). Previous studies demonstrate that NF-κB activation can synergize with MYC overexpression or *Pten* heterozygosity to accelerate murine prostate cancer initiation and the NF-κB activation signature in human tumors can predict poor outcome (Birbach et al., 2011; Jin et al., 2014). These data suggest that NF-κB activity may predispose CD38^{lo} luminal cells to tumor initiation. More work is necessary to determine whether strategies to reduce inflammation or small molecules that block epithelial NF-κB signaling can prevent prostate cancer initiation by targeting CD38^{lo} luminal cell survival and progenitor activity.

CD38^{lo} luminal cells express PSCA, which is being evaluated as a therapeutic target in clinical trials using monoclonal antibodies (Morris et al., 2012). BCL2 expression in CD38^{lo} luminal cells may enhance their resistance to apoptosis (Raffo et al., 1995). Both BCL2 and PSCA are associated with castration resistance (Gu et al., 2000; Raffo et al., 1995), suggesting that CD38^{lo} luminal cells may have a survival advantage under low-androgen conditions. Consistent with mouse models demonstrating that prostatic inflammation or epithelial NF-κB activation is associated with reduced androgen signaling and increased epithelial proliferation (Birbach et al., 2011; Khalili et al., 2010), CD38^{lo} luminal cells express low levels of PSA and other androgen targets. These data suggest that CD38^{lo} luminal-like cancer cells may contribute to castration-resistant prostate cancer.

Distinguishing indolent from aggressive prostate cancer remains a critical goal of the field. We found that low expression of CD38 mRNA in prostatectomy specimens is prognostic for biochemical recurrence in two independent cohorts (Figures 5C–5E). These data suggest that aggressive tumors may arise in CD38^{lo} luminal cells that retain low expression of CD38.

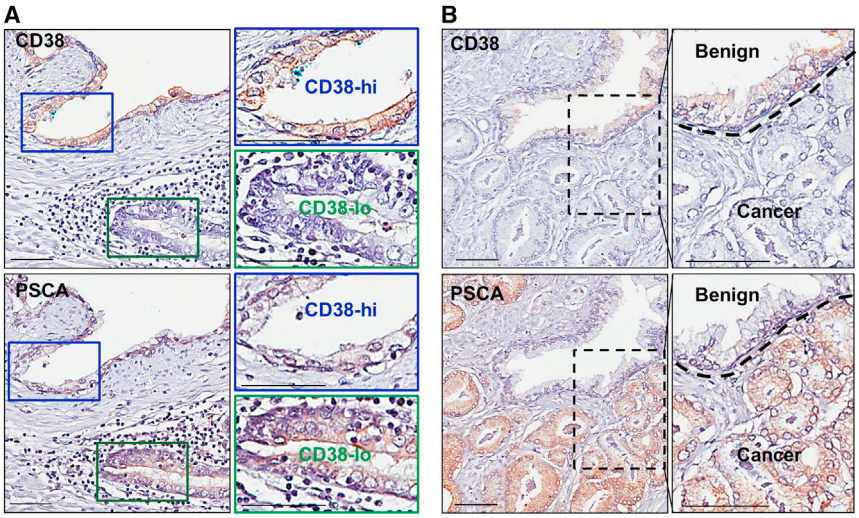

Figure 6. PSCA Is Expressed in CD38^{lo} Luminal Cells

(A) Serial sections of benign human prostate stained for CD38 and PSCA with boxed regions to magnify distinct CD38^{hi} PSCA-lo glands and inflammation-associated CD38^{lo} PSCA-hi cells.

(B) Serial sections of human prostate tissue stained for CD38 and PSCA with boxed region magnifying CD38^{hi} PSCA-lo benign tissue separated by a dotted line from CD38^{lo} PSCA-hi cancer. Scale bars, 50 μm.

Alternatively, the activation of a CD38^{lo} luminal-like signature during tumorigenesis may promote an aggressive phenotype, regardless of the cell of origin. Several studies have looked at the cellular origins of cancer to distinguish indolent from aggressive prostate cancer with different results using distinct mouse models (Choi et al., 2012; Lu et al., 2013; Wang et al., 2009, 2013, 2014). In human prostate models, basal cells have been shown to generate aggressive, highly proliferative tumors, while luminal cells can initiate only indolent tumors (Goldstein et al., 2010; Park et al., 2016; Stoyanova et al., 2013). In this study, we demonstrate that CD38^{lo} luminal cells can generate highly proliferative prostate cancer (>40% Ki67+). Taken together, we hypothesize that one target cell (basal) is predisposed to the initiation of aggressive cancer under normal conditions. In the context of chronic inflammation, a second target cell (CD38^{lo} luminal) is predisposed to initiate aggressive cancer, perhaps due to elevated NF-κB signaling.

CD38^{lo} luminal cells may arise from basal to luminal differentiation, as has been demonstrated using lineage tracing in mouse models of inflammation (Kwon et al., 2014, 2016). Alternatively, inflammation may alter the differentiation of luminal cells by enhancing NF-κB signaling and reducing androgen signaling. Future studies will determine whether exposure to inflammatory cytokines can reprogram CD38^{hi} luminal cells into a progenitor-enriched CD38^{lo} luminal-like cell capable of initiating aggressive prostate cancer. Interestingly, CD38^{lo} luminal cells express cytokines and chemokines known to recruit pro-inflammatory cells and promote tumorigenesis in other tissues like *Ccl2* (Qian et al., 2011) and *Cxcl1/2* (Jablonska et al., 2014), indicating that CD38^{lo} luminal cells may influence their microenvironment to promote inflammation and maintain proliferative cues.

Our findings are consistent with previous reports of low CD38 expression in prostate cancer (Kramer et al., 1995; Pascal et al., 2009). While rare deletions and mutations of CD38 can be identified in metastatic castration-resistant prostate cancer (Grasso et al., 2012; Robinson et al., 2015), transcriptional repression of CD38 is the likely mechanism causing low expression in the vast majority of prostate tumors. CD38 is an ectoenzyme that consumes the cofactor nicotinamide adenine dinucleotide (NAD) (Howard et al., 1993), suggesting that loss of CD38 may serve to increase pools of NAD required for cellular metabolism in prostate cancer. Further study of the functional role of CD38 in tumorigenesis and the cellular mechanisms driving CD38^{lo} luminal cells may yield new predictive markers and therapeutic targets for aggressive disease.

EXPERIMENTAL PROCEDURES

qPCR, RNA Sequencing, Bioinformatics, and Microarray

RNA was extracted from cell pellets using the RNeasy mini Kit (QIAGEN/SA Biosciences). qPCR was carried out as previously described (Goldstein et al., 2010) using commercial primers to *Gapdh*, *Keratin 8*, and *Klk3* (QIAGEN/SA Biosciences). RNA-seq libraries were prepared with the Ovation RNA-Seq System V2 (Nugen). Double-stranded cDNA was generated with a mixture of random and poly(T) priming, followed by fragmentation, generation of blunt ends by end repair, A-tailing, ligation of adaptors (different adaptors for multiplexing samples), PCR amplification, and sequencing (pair read 100 run) on Illumina HiSeq 2500. Illumina SAV was used for data quality check, and Illumina CASAVA 1.8.2 was used for de-multiplexing. Reads were mapped to the most recent UCSC transcript set with Bowtie2 version 2.1.0. RSEM v1.2.15 was used to estimate level of gene expression. Gene expression was normalized by TPM (transcript per million) or RPKM (reads per kilobase per million mapped reads). DeSeq was used to identify differentially expressed genes. FASTQ files were not available at the time of publication. For that reason, the full RPKM values are provided in Table S1. Upstream regulator analysis was performed using QIAGEN's Ingenuity Pathway Analysis (http://www.ingenuity.com). For microarray analysis, total RNA was isolated from sorted cells with RNeasy Micro Kit and amplified with NuGen Pico kit according to standard manufacturer protocols. Biotinylated cDNA were prepared from total RNA using the standard Affymetrix protocol and hybridized to the Affymetrix Human Genome U133 Plus 2.0 Chip. Chips were scanned using an Affymetrix GeneChip Scanner 7G and data were analyzed with Microarray Suite version 5.0 (MAS 5.0) using Affymetrix default analysis settings and global scaling as normalization method. Data are available at the GEO repository under accession number GEO: GSE89050.

Primary Cell Preparation and Cell Separation

Human prostate tissue samples were provided in a de-identified manner deemed by the institutional review board to not qualify as human subjects. Tissue was provided by the UCLA Translational Pathology Core Laboratory, and benign specimens were processed as described in detail previously (Goldstein et al., 2011). For antibody staining of primary benign dissociated cells, see Supplemental Information). Intracellular flow cytometry has been described previously (Goldstein et al., 2010). Antibodies are listed in Supplemental Information.

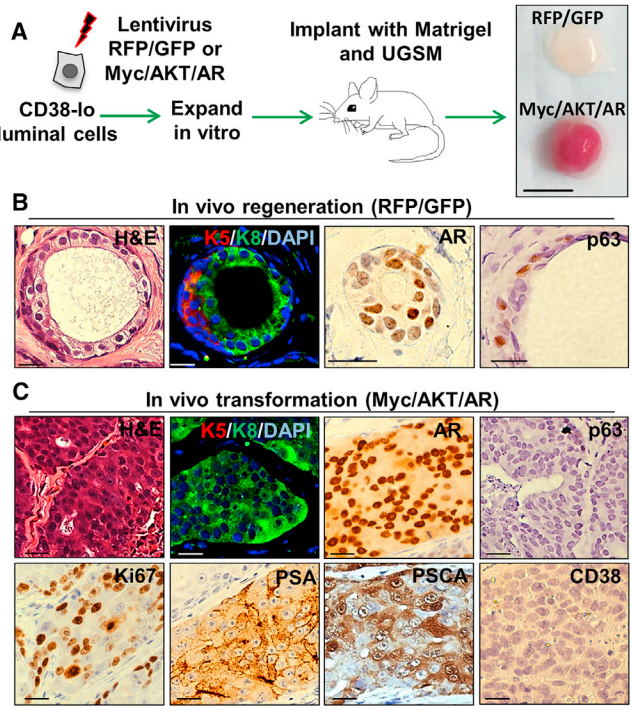

Figure 7. CD38^{lo} Luminal Cells Can Generate Glands and Initiate Human Prostate Cancer In Vivo

(A) Schematic representing experimental flow where CD38^{lo} luminal cells are transduced with lentivirus, expanded in vitro 7–10 days, combined with UGSM and Matrigel and implanted in vivo. Regenerated tissues from representative experiments are shown on the right. Scale bars, 5 mm.

(B) Representative in vivo regeneration of CD38^{lo} luminal cell-derived organoids transduced with control fluorescent GFP and red fluorescent protein (RFP) stained for H&E, K5, K8, DAPI nuclear counterstain, AR, and p63. Scale bars, 50 μm.

(C) Representative adenocarcinoma in regenerated tumor tissues from CD38^{lo} luminal cells transduced with Myc, AKT, and AR stained for H&E, K5, K8, DAPI nuclear counterstain, AR, p63, Ki67, PSA, PSCA, and CD38. Scale bars, 25 μm.

Immunohistochemical Analysis and Immunofluorescence

Paraffin-embedded tissue sections were incubated in a 60°C oven for 1 hr and de-paraffinized in three changes of xylene, followed by 100% alcohol twice for 3 min each. Then the slides were transferred once in 95% and 70% alcohol, each for 3 min. A heat antigen retrieval step was used to unmask the antigenic epitopes. The remaining procedure was performed according to the manufacturer's protocol (R&D Cell and Tissue Staining Kit HRP-DAB system, R&D Systems). Primary antibodies are listed in Supplemental Information. Biotinylated anti-mouse and anti-rabbit secondary antibodies are supplied by HRP-DAB system for Mouse (CTS002, R&D Systems) and Rabbit Kit (CTS005, R&D Systems). Double-sorted cells were plated onto a glass slide coated with poly-L-lysine (Sigma), and cells were allowed to attach overnight. The following day, cells were fixed in 4% paraformaldehyde, washed three times in 1× PBS and stained with primary antibody. Alexa-488-conjugated goat anti-mouse secondary antibody (A-11001, Invitrogen) was used followed by DAPI nuclear counterstain (H-1200, Vector Laboratories).

Immunoblot Analysis

Isolated cell populations were lysed in RIPA buffer (150mM NaCl, 1% NP-40, 50 mM Tris-HCl [pH 8.0], 0.5% sodium deoxycholate, and 0.1% SDS) with protease inhibitor cocktail tablet (Complete, Roche) on ice 15 min followed by spin at maximum speed for 15 min. Supernatants were boiled in loading buffer and membranes probed with antibodies (see Supplemental Information). Primary rabbit, mouse, or goat antibodies were detected with horseradish peroxidase (HRP)-conjugated secondary antibodies (Pierce).

Tissue Microarray and Scoring

The tissue microarray was constructed from 332 men who underwent radical prostatectomy surgery at the West Los Angeles Veteran's Administration Hospital from 1991 to 2003 and has been described previously (Gollapudi et al., 2013). At least three cores of each histological type are included per patient. Follow-up patient information for up to 120 months was used for analysis. Biochemical recurrence refers to PSA values greater than 0.2, two readings at 0.2, or additional treatment for high post-operative PSA. 4-μm sections were stained for CD38 and scanned using the Aperioslide scanner, and staining was evaluated in a blinded fashion by the pathologists (B.N. and J.H.). Scoring was assessed based on staining intensity from 0 (no staining) to 3 (strong) and percentage of tumor cell expression (1%–100%), creating a composite score from 0 to 300. For statistical methods, see Supplemental Information.

Cell Culture

For the in vitro organoid-forming assay, double-sorted FACS-isolated cell populations were plated in a 96-well plate (Corning Incorporated) at a cell density of one cell per well, and those wells with a single cell were visually confirmed and marked for continued analysis. Prostate organoid growth conditions were based on established protocols (Karthaus et al., 2014). Primary single-cell organoids were dissociated in 1 mg/mL Dispase (Gibco) at 37°C for 1 hr and then treated with 0.05% Trypsin-EDTA (Life Technologies) in order to passage. For the colony assay, primary cells were plated on Matrigel-coated six-well dishes as described previously (Lukacs et al., 2010) and grown in PrEGM media. Colonies containing more than two cells were quantified after 10–14 days. For the sphere assay, cells were resuspended in a PrEGM/Matrigel mixture and plated around the edges of the well in a 12-well dish as described previously (Lukacs et al., 2010). Spheres were quantified after 10–14 days. For inhibition of NF-κB, ACHP (4547, Tocris) was added to organoid media at a final concentration of 5 μM every 3 days.

In Vivo Regeneration and Transformation and Animal Care

In vivo tissue-regeneration and transformation methods have been described in detail (Goldstein et al., 2011). Transduced cells were expanded in organoid culture (Karthaus et al., 2014) prior to transplantation as described previously (Park et al., 2016). All human tissues were transplanted subcutaneously into NOD-SCID-IL2Rγ^{null} mice. Animals have been purchased from the Jackson Laboratory and are now housed and bred under the care of the Division of Laboratory Animal Medicine at the University of California, Los Angeles, using protocols approved by the Animal Research Committee. Lentiviral vectors were previously described (Goldstein et al., 2010; Stoyanova et al., 2013).

ACCESSION NUMBERS

The accession number for the data reported in this paper is GEO: GSE89050.

SUPPLEMENTAL INFORMATION

Supplemental Information includes Supplemental Experimental Procedures, seven figures, and six tables and can be found with this article online at http://dx.doi.org/10.1016/j.celrep.2016.11.010.

AUTHOR CONTRIBUTIONS

X.L. and A.S.G. performed the majority of experiments and wrote and edited the manuscript. T.H., J.M., D.C., L.Z., K.H., T.S., and R.O.S. performed experiments. T.R.G., D.E., S.H., H.H., and C.L.S. performed statistical analysis. J.W.P. developed organoid transformation methods. B.N. and J.H. provided pathology expertise. M.B.R. provided tissue microarrays. J.H. and O.N.W. edited and contributed to writing of the manuscript.

ACKNOWLEDGMENTS

This work was supported by Department of Defense Idea Development Award W81XWH-13-1-0470 (A.S.G. and S.H.), a Prostate Cancer Foundation Young Investigator Award (A.S.G. and T.S.), the Broad Stem Cell Research Center (A.S.G. and J.H.), an AACR/PCF/Stand Up 2 Cancer West Coast Dream Team Award (O.N.W., J.H., M.R., and A.S.G.), a National Institute of Health/National Cancer Institute grant (P50CA092131/UCLA SPORE in Prostate Cancer; D.E., S.H., O.N.W., J.H., M.R., and A.S.G), a NIH/National Center for Advancing Translational Science (NCATS) UCLA CTSI grant (UL1TR000124; T.R.G. and D.E.), a National Institute of Health/National Cancer Institute K99 Pathway to Independence Award (4R00CA184397; T.S.), and the Howard Hughes Medical Institute (O.N.W.). M.R. and funding for TMA creation were supported by the Department of Defense (PC030686).

Received: June 17, 2016
Revised: September 27, 2016
Accepted: October 28, 2016
Published: December 6, 2016

REFERENCES

Ammirante, M., Luo, J.L., Grivennikov, S., Nedospasov, S., and Karin, M. (2010). B-cell-derived lymphotoxin promotes castration-resistant prostate cancer. Nature *464*, 302–305.

Birbach, A., Eisenbarth, D., Kozakowski, N., Ladenhauf, E., Schmidt-Supprian, M., and Schmid, J.A. (2011). Persistent inflammation leads to proliferative neoplasia and loss of smooth muscle cells in a prostate tumor model. Neoplasia *13*, 692–703.

Choi, N., Zhang, B., Zhang, L., Ittmann, M., and Xin, L. (2012). Adult murine prostate basal and luminal cells are self-sustained lineages that can both serve as targets for prostate cancer initiation. Cancer Cell *21*, 253–265.

Coussens, L.M., and Werb, Z. (2002). Inflammation and cancer. Nature *420*, 860–867.

Das Roy, L., Pathangey, L.B., Tinder, T.L., Schettini, J.L., Gruber, H.E., and Mukherjee, P. (2009). Breast-cancer-associated metastasis is significantly increased in a model of autoimmune arthritis. Breast Cancer Res. *11*, R56.

De Marzo, A.M., Marchi, V.L., Epstein, J.I., and Nelson, W.G. (1999). Proliferative inflammatory atrophy of the prostate: implications for prostatic carcinogenesis. Am. J. Pathol. *155*, 1985–1992.

De Marzo, A.M., Meeker, A.K., Zha, S., Luo, J., Nakayama, M., Platz, E.A., Isaacs, W.B., and Nelson, W.G. (2003). Human prostate cancer precursors and pathobiology. Urology *62* (*5, Suppl 1*), 55–62.

De Marzo, A.M., Platz, E.A., Sutcliffe, S., Xu, J., Grönberg, H., Drake, C.G., Nakai, Y., Isaacs, W.B., and Nelson, W.G. (2007). Inflammation in prostate carcinogenesis. Nat. Rev. Cancer *7*, 256–269.

Elkahwaji, J.E., Hauke, R.J., and Brawner, C.M. (2009). Chronic bacterial inflammation induces prostatic intraepithelial neoplasia in mouse prostate. Br. J. Cancer *101*, 1740–1748.

Garcia, A.J., Ruscetti, M., Arenzana, T.L., Tran, L.M., Bianci-Frias, D., Sybert, E., Priceman, S.J., Wu, L., Nelson, P.S., Smale, S.T., and Wu, H. (2014). Pten null prostate epithelium promotes localized myeloid-derived suppressor cell expansion and immune suppression during tumor initiation and progression. Mol. Cell. Biol. *34*, 2017–2028.

Goldstein, A.S., Lawson, D.A., Cheng, D., Sun, W., Garraway, I.P., and Witte, O.N. (2008). Trop2 identifies a subpopulation of murine and human prostate basal cells with stem cell characteristics. Proc. Natl. Acad. Sci. USA *105*, 20882–20887.

Goldstein, A.S., Huang, J., Guo, C., Garraway, I.P., and Witte, O.N. (2010). Identification of a cell of origin for human prostate cancer. Science *329*, 568–571.

Goldstein, A.S., Drake, J.M., Burnes, D.L., Finley, D.S., Zhang, H., Reiter, R.E., Huang, J., and Witte, O.N. (2011). Purification and direct transformation of epithelial progenitor cells from primary human prostate. Nat. Protoc. *6*, 656–667.

Gollapudi, K., Galet, C., Grogan, T., Zhang, H., Said, J.W., Huang, J., Elashoff, D., Freedland, S.J., Rettig, M., and Aronson, W.J. (2013). Association between tumor-associated macrophage infiltration, high grade prostate cancer, and biochemical recurrence after radical prostatectomy. Am. J. Cancer Res. *3*, 523–529.

Grasso, C.S., Wu, Y.M., Robinson, D.R., Cao, X., Dhanasekaran, S.M., Khan, A.P., Quist, M.J., Jing, X., Lonigro, R.J., Brenner, J.C., et al. (2012). The mutational landscape of lethal castration-resistant prostate cancer. Nature *487*, 239–243.

Gu, Z., Thomas, G., Yamashiro, J., Shintaku, I.P., Dorey, F., Raitano, A., Witte, O.N., Said, J.W., Loda, M., and Reiter, R.E. (2000). Prostate stem cell antigen (PSCA) expression increases with high gleason score, advanced stage and bone metastasis in prostate cancer. Oncogene *19*, 1288–1296.

Gurel, B., Lucia, M.S., Thompson, I.M., Jr., Goodman, P.J., Tangen, C.M., Kristal, A.R., Parnes, H.L., Hoque, A., Lippman, S.M., Sutcliffe, S., et al. (2014). Chronic inflammation in benign prostate tissue is associated with high-grade prostate cancer in the placebo arm of the prostate cancer prevention trial. Cancer Epidemiol. Biomarkers Prev. *23*, 847–856.

Haverkamp, J.M., Charbonneau, B., Crist, S.A., Meyerholz, D.K., Cohen, M.B., Snyder, P.W., Svensson, R.U., Henry, M.D., Wang, H.H., and Ratliff, T.L. (2011). An inducible model of abacterial prostatitis induces antigen specific inflammatory and proliferative changes in the murine prostate. Prostate *71*, 1139–1150.

Hieronymus, H., Lamb, J., Ross, K.N., Peng, X.P., Clement, C., Rodina, A., Nieto, M., Du, J., Stegmaier, K., Raj, S.M., et al. (2006). Gene expression signature-based chemical genomic prediction identifies a novel class of HSP90 pathway modulators. Cancer Cell *10*, 321–330.

Hieronymus, H., Schultz, N., Gopalan, A., Carver, B.S., Chang, M.T., Xiao, Y., Heguy, A., Huberman, K., Bernstein, M., Assel, M., et al. (2014). Copy number alteration burden predicts prostate cancer relapse. Proc. Natl. Acad. Sci. USA *111*, 11139–11144.

Howard, M., Grimaldi, J.C., Bazan, J.F., Lund, F.E., Santos-Argumedo, L., Parkhouse, R.M., Walseth, T.F., and Lee, H.C. (1993). Formation and hydrolysis of cyclic ADP-ribose catalyzed by lymphocyte antigen CD38. Science *262*, 1056–1059.

Huang da, W., Sherman, B.T., and Lempicki, R.A. (2009). Systematic and integrative analysis of large gene lists using DAVID bioinformatics resources. Nat. Protoc. *4*, 44–57.

Jablonska, J., Wu, C.F., Andzinski, L., Leschner, S., and Weiss, S. (2014). CXCR2-mediated tumor-associated neutrophil recruitment is regulated by IFN-β. Int. J. Cancer *134*, 1346–1358.

Jin, R., Yi, Y., Yull, F.E., Blackwell, T.S., Clark, P.E., Koyama, T., Smith, J.A., Jr., and Matusik, R.J. (2014). NF-κB gene signature predicts prostate cancer progression. Cancer Res. *74*, 2763–2772.

Karthaus, W.R., Iaquinta, P.J., Drost, J., Gracanin, A., van Boxtel, R., Wongvipat, J., Dowling, C.M., Gao, D., Begthel, H., Sachs, N., et al. (2014). Identification of multipotent luminal progenitor cells in human prostate organoid cultures. Cell *159*, 163–175.

Khalili, M., Mutton, L.N., Gurel, B., Hicks, J.L., De Marzo, A.M., and Bieberich, C.J. (2010). Loss of Nkx3.1 expression in bacterial prostatitis: a potential link between inflammation and neoplasia. Am. J. Pathol. *176*, 2259–2268.

Kramer, G., Steiner, G., Födinger, D., Fiebiger, E., Rappersberger, C., Binder, S., Hofbauer, J., and Marberger, M. (1995). High expression of a CD38-like molecule in normal prostatic epithelium and its differential loss in benign and malignant disease. J. Urol. *154*, 1636–1641.

Kwon, O.J., Zhang, L., Ittmann, M.M., and Xin, L. (2014). Prostatic inflammation enhances basal-to-luminal differentiation and accelerates initiation of prostate cancer with a basal cell origin. Proc. Natl. Acad. Sci. USA *111*, E592–E600.

Kwon, O.J., Zhang, B., Zhang, L., and Xin, L. (2016). High fat diet promotes prostatic basal-to-luminal differentiation and accelerates initiation of prostate

epithelial hyperplasia originated from basal cells. Stem Cell Res. (Amst.) *16*, 682–691.

Lawson, D.A., Zong, Y., Memarzadeh, S., Xin, L., Huang, J., and Witte, O.N. (2010). Basal epithelial stem cells are efficient targets for prostate cancer initiation. Proc. Natl. Acad. Sci. USA *107*, 2610–2615.

Liu, K., Jiang, M., Lu, Y., Chen, H., Sun, J., Wu, S., Ku, W.Y., Nakagawa, H., Kita, Y., Natsugoe, S., et al. (2013). Sox2 cooperates with inflammation-mediated Stat3 activation in the malignant transformation of foregut basal progenitor cells. Cell Stem Cell *12*, 304–315.

Lu, T.L., Huang, Y.F., You, L.R., Chao, N.C., Su, F.Y., Chang, J.L., and Chen, C.M. (2013). Conditionally ablated Pten in prostate basal cells promotes basal-to-luminal differentiation and causes invasive prostate cancer in mice. Am. J. Pathol. *182*, 975–991.

Lukacs, R.U., Goldstein, A.S., Lawson, D.A., Cheng, D., and Witte, O.N. (2010). Isolation, cultivation and characterization of adult murine prostate stem cells. Nat. Protoc. *5*, 702–713.

Morris, M.J., Eisenberger, M.A., Pili, R., Denmeade, S.R., Rathkopf, D., Slovin, S.F., Farrelly, J., Chudow, J.J., Vincent, M., Scher, H.I., and Carducci, M.A. (2012). A phase I/IIA study of AGS-PSCA for castration-resistant prostate cancer. Ann. Oncol. *23*, 2714–2719.

Nelson, P.S., Clegg, N., Arnold, H., Ferguson, C., Bonham, M., White, J., Hood, L., and Lin, B. (2002). The program of androgen-responsive genes in neoplastic prostate epithelium. Proc. Natl. Acad. Sci. USA *99*, 11890–11895.

Network, T.R.; Cancer Genome Atlas Research Network (2015). The molecular taxonomy of primary prostate cancer. Cell *163*, 1011–1025.

Park, J.W., Lee, J.K., Phillips, J.W., Huang, P., Cheng, D., Huang, J., and Witte, O.N. (2016). Prostate epithelial cell of origin determines cancer differentiation state in an organoid transformation assay. Proc. Natl. Acad. Sci. USA *113*, 4482–4487.

Pascal, L.E., Vêncio, R.Z., Page, L.S., Liebeskind, E.S., Shadle, C.P., Troisch, P., Marzolf, B., True, L.D., Hood, L.E., and Liu, A.Y. (2009). Gene expression relationship between prostate cancer cells of Gleason 3, 4 and normal epithelial cells as revealed by cell type-specific transcriptomes. BMC Cancer *9*, 452.

Qian, B.Z., Li, J., Zhang, H., Kitamura, T., Zhang, J., Campion, L.R., Kaiser, E.A., Snyder, L.A., and Pollard, J.W. (2011). CCL2 recruits inflammatory monocytes to facilitate breast-tumour metastasis. Nature *475*, 222–225.

Raffo, A.J., Perlman, H., Chen, M.W., Day, M.L., Streitman, J.S., and Buttyan, R. (1995). Overexpression of bcl-2 protects prostate cancer cells from apoptosis in vitro and confers resistance to androgen depletion in vivo. Cancer Res. *55*, 4438–4445.

Robinson, D., Van Allen, E.M., Wu, Y.M., Schultz, N., Lonigro, R.J., Mosquera, J.M., Montgomery, B., Taplin, M.E., Pritchard, C.C., Attard, G., et al. (2015). Integrative clinical genomics of advanced prostate cancer. Cell *161*, 1215–1228.

Sato, T., Vries, R.G., Snippert, H.J., van de Wetering, M., Barker, N., Stange, D.E., van Es, J.H., Abo, A., Kujala, P., Peters, P.J., and Clevers, H. (2009). Single Lgr5 stem cells build crypt-villus structures in vitro without a mesenchymal niche. Nature *459*, 262–265.

Sboner, A., Demichelis, F., Calza, S., Pawitan, Y., Setlur, S.R., Hoshida, Y., Perner, S., Adami, H.O., Fall, K., Mucci, L.A., et al. (2010). Molecular sampling of prostate cancer: a dilemma for predicting disease progression. BMC Med. Genomics *3*, 8.

Sfanos, K.S., and De Marzo, A.M. (2012). Prostate cancer and inflammation: the evidence. Histopathology *60*, 199–215.

Shafique, K., Proctor, M.J., McMillan, D.C., Qureshi, K., Leung, H., and Morrison, D.S. (2012). Systemic inflammation and survival of patients with prostate cancer: evidence from the Glasgow Inflammation Outcome Study. Prostate Cancer Prostatic Dis. *15*, 195–201.

Smith, B.A., Sokolov, A., Uzunangelov, V., Baertsch, R., Newton, Y., Graim, K., Mathis, C., Cheng, D., Stuart, J.M., and Witte, O.N. (2015). A basal stem cell signature identifies aggressive prostate cancer phenotypes. Proc. Natl. Acad. Sci. USA *112*, E6544–E6552.

Stephenson, A.J., Scardino, P.T., Eastham, J.A., Bianco, F.J., Jr., Dotan, Z.A., DiBlasio, C.J., Reuther, A., Klein, E.A., and Kattan, M.W. (2005). Postoperative nomogram predicting the 10-year probability of prostate cancer recurrence after radical prostatectomy. J. Clin. Oncol. *23*, 7005–7012.

Stoyanova, T., Cooper, A.R., Drake, J.M., Liu, X., Armstrong, A.J., Pienta, K.J., Zhang, H., Kohn, D.B., Huang, J., Witte, O.N., and Goldstein, A.S. (2013). Prostate cancer originating in basal cells progresses to adenocarcinoma propagated by luminal-like cells. Proc. Natl. Acad. Sci. USA *110*, 20111–20116.

Taylor, B.S., Schultz, N., Hieronymus, H., Gopalan, A., Xiao, Y., Carver, B.S., Arora, V.K., Kaushik, P., Cerami, E., Reva, B., et al. (2010). Integrative genomic profiling of human prostate cancer. Cancer Cell *18*, 11–22.

Taylor, R.A., Toivanen, R., Frydenberg, M., Pedersen, J., Harewood, L., Collins, A.T., Maitland, N.J., and Risbridger, G.P.; Australian Prostate Cancer Bioresource (2012). Human epithelial basal cells are cells of origin of prostate cancer, independent of CD133 status. Stem Cells *30*, 1087–1096.

van Leenders, G.J., Gage, W.R., Hicks, J.L., van Balken, B., Aalders, T.W., Schalken, J.A., and De Marzo, A.M. (2003). Intermediate cells in human prostate epithelium are enriched in proliferative inflammatory atrophy. Am. J. Pathol. *162*, 1529–1537.

Wang, X., Kruithof-de Julio, M., Economides, K.D., Walker, D., Yu, H., Halili, M.V., Hu, Y.P., Price, S.M., Abate-Shen, C., and Shen, M.M. (2009). A luminal epithelial stem cell that is a cell of origin for prostate cancer. Nature *461*, 495–500.

Wang, Z.A., Mitrofanova, A., Bergren, S.K., Abate-Shen, C., Cardiff, R.D., Califano, A., and Shen, M.M. (2013). Lineage analysis of basal epithelial cells reveals their unexpected plasticity and supports a cell-of-origin model for prostate cancer heterogeneity. Nat. Cell Biol. *15*, 274–283.

Wang, Z.A., Toivanen, R., Bergren, S.K., Chambon, P., and Shen, M.M. (2014). Luminal cells are favored as the cell of origin for prostate cancer. Cell Rep. *8*, 1339–1346.

Wang, D., Fu, L., Sun, H., Guo, L., and DuBois, R.N. (2015). Prostaglandin E2 promotes colorectal cancer stem cell expansion and metastasis in mice. Gastroenterology *149*, 1884–1895.

Cell Reports, Volume *17*

Supplemental Information

Low CD38 Identifies Progenitor-like Inflammation-Associated Luminal Cells that Can Initiate Human Prostate Cancer and Predict Poor Outcome

Xian Liu, Tristan R. Grogan, Haley Hieronymus, Takao Hashimoto, Jack Mottahedeh, Donghui Cheng, Lijun Zhang, Kevin Huang, Tanya Stoyanova, Jung Wook Park, Ruzanna O. Shkhyan, Behdokht Nowroozizadeh, Matthew B. Rettig, Charles L. Sawyers, David Elashoff, Steve Horvath, Jiaoti Huang, Owen N. Witte, and Andrew S. Goldstein

Supplemental Information

Low CD38 identifies progenitor-like inflammation-associated luminal cells that can initiate human prostate cancer and predict poor outcome

Xian Liu, Tristan R. Grogan, Haley Hieronymus, Takao Hashimoto, Jack Mottahedeh, Donghui Cheng, Lijun Zhang, Kevin Huang, Tanya Stoyanova, Jung Wook Park, Ruzanna O. Shkhyan, Behdokht Nowroozizadeh, Matthew B. Rettig, Charles L. Sawyers, David Elashoff, Steve Horvath, Jiaoti Huang, Owen N. Witte, Andrew S. Goldstein

Supplemental Text

Experimental Procedures

Comparison of CD38 expression between histological grades

To compare the CD38 expression levels between the four different prostate regions (Normal, PIN, Gleason < 7, Gleason 7-10), a generalized estimating equation (GEE) model was run with the normal/identity link function. We performed a log+1 transformation prior to analysis due to the skewed distribution of the score. The exchangeable correlation structure was used in the model to account for repeated measures (i.e. multiple cores per person). After the overall effect of different levels of CD38 among the prostate regions was confirmed ($p<0.001$), follow-up pairwise comparisons were run to determine which regions were statistically significantly different from one another. To control the overall familywise error rate at $\alpha=0.05$ we used Tukey's adjusted p-values for multiple comparisons.

Summary measure for CD38

Before constructing a prognostic model with CD38 as a predictor, the correlation between the scores across the different histological grades was assessed. The correlation between the average CD38 expression between normal, PIN, and cancer cores was computed using Spearman's rank correlation coefficient. The correlations between the 3 regions were fairly low (between 0.20-0.30) indicating some biological variation across the different core sample types within an individual. In general the cancer cores expressed lower CD38 levels compared to the PIN and normal regions (Figure 5C). Cox proportional-hazards models were used to determine the prognostic ability of CD38 as a predictor of biochemical recurrence. A statistically significant association between overall mean (low) expression of CD38 and time to biochemical recurrence was observed ($p=0.025$). All analyses were performed in SAS V9.4 (SAS Institute, Cary, NC) and SPSS V22 (IBM Corp., Armonk, NY). P-values <0.05 were considered statistically significant.

Antibodies used

FACS and flow cytometry: CD45-APC-eFluor® 780 (47-0459-41, eBiosciences), EpCAM-APC (324207, BioLegend), CD49f-PEcy7 (313621, BioLegend), CD38-PE (303505, BioLegend) and CD26-FITC (302705, BioLegend), Keratin 18-FITC antibody (ab72813, Abcam) Keratin 5-FITC (FCMAB291F, Millipore).

Immunohistochemistry: CD38 (LS-B8131, Lifespan Biosciences; sc-374650, Santa Cruz), CD45 (M0701, Dako), CD4 (MS-1528, Thermo Scientific), CD8 (M7103, Dako), CD11c (ab52632, Abcam), CD68 (M0876, Dako), CD20 (M0755, Dako), CD26 (LS-A9024, Lifespan Biosciences), Keratin 5 (905501, Biolegend), Keratin 8 (904801, BioLegend), p63 (sc-8431, Santa Cruz), AR (M3562, Dako), PSA (A0562, Dako), FKBP5 (ab126715, Abcam), MSMB (ab133296, Abcam), PSCA (LS-B3332, Lifespan Biosciences), NF-kB p65 phosphorylated S536 (ab86299, Abcam), TNF alpha (60291-1-Ig, Proteintech), Myc (ab32072, Abcam), phospho-AKT (3787, Cell Signaling), Ki67 (M7240, Dako), Nkx3-1 (0314, Athena Environmental Sciences).

Immunoblot: p63 (sc-8431, Santa Cruz), CD38 (sc-374650, Santa Cruz), K14 (905301, BioLegend), Histone H3 (9715, Cell Signaling), AR (sc-816, Santa Cruz), NF-kB p65 (ab31481, Abcam), NF-kB p65 phosphorylated S536 (ab86299, Abcam), BCL2 (M0887, Dako).

Supplemental Figures

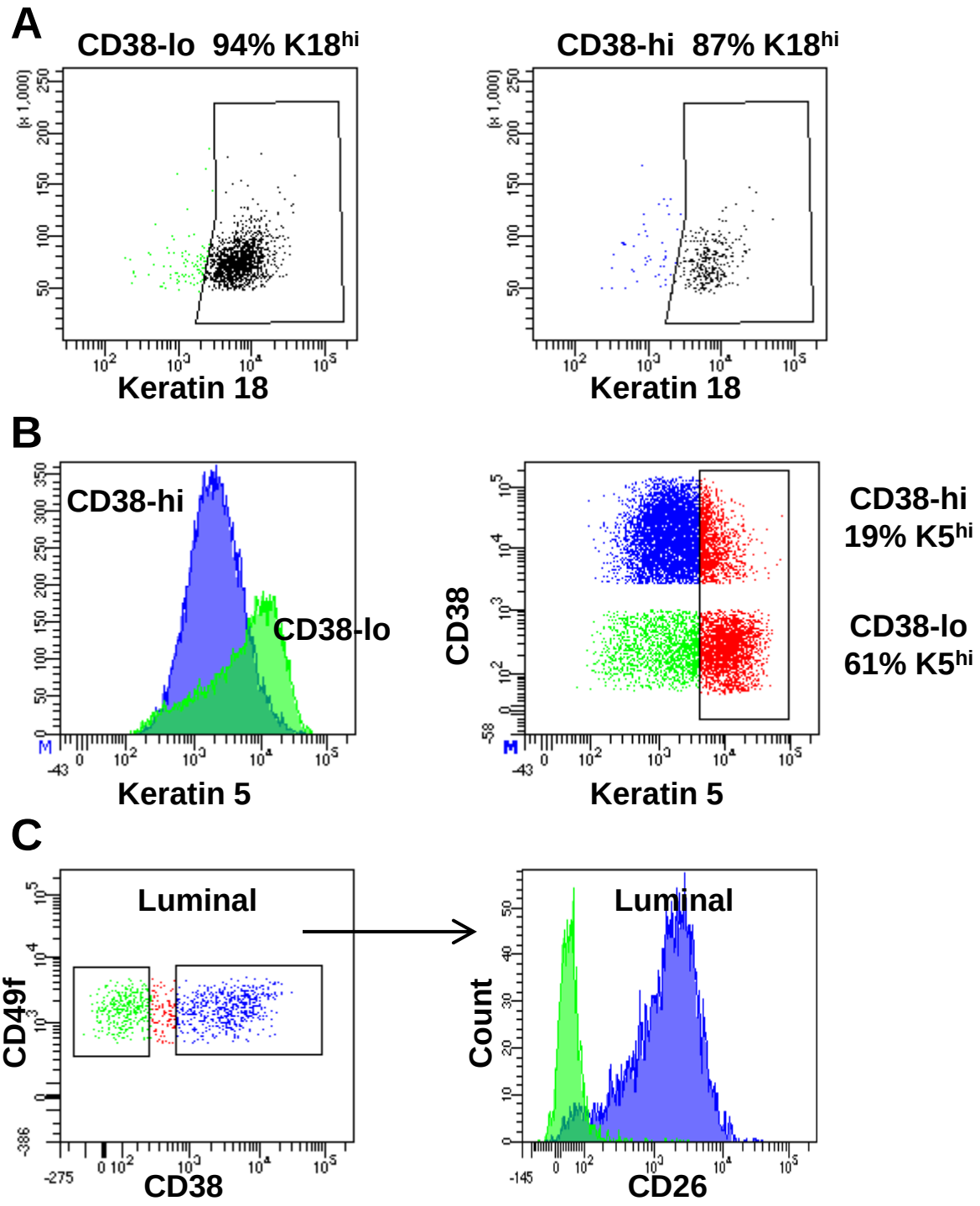

Fig. S1. Expression of keratins and CD26 in CD38-hi and CD38-lo luminal cells, related to Figure 1. (A-B) Intracellular flow cytometry on benign human prostate glands, gated on CD45- EpCAM+ CD49f-lo luminal cells, further stratified into CD38-hi and CD38-lo subsets and stained with antibodies against Keratin-18 (A) or Keratin-5 (B). (C) Flow cytometry on benign human prostate glands stained with antibodies against CD45, EpCAM, CD49f, CD38 and CD26. CD45- EpCAM+ CD49f-low CD38-low luminal cells do not express CD26.

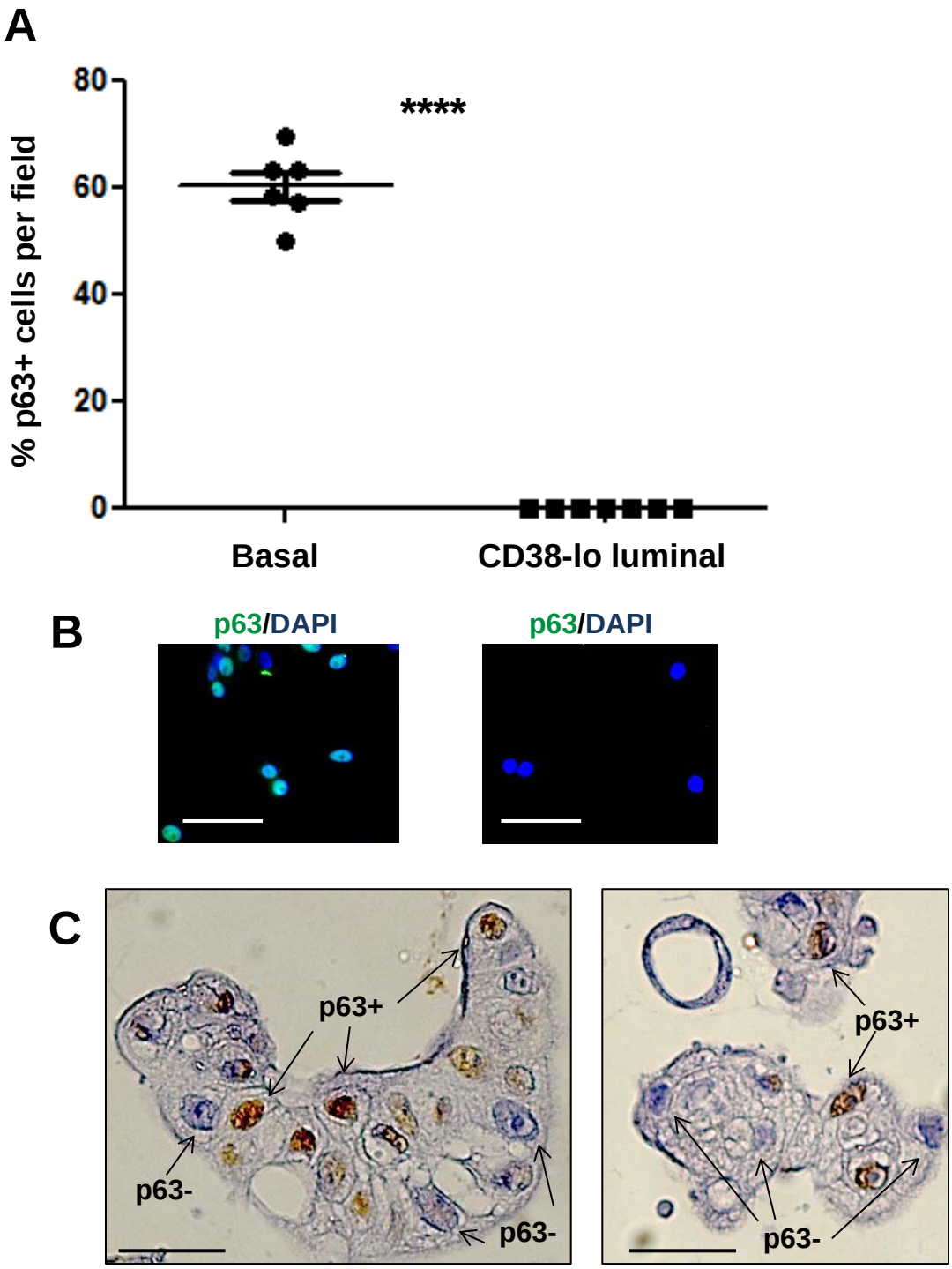

Fig. S2. p63 expression is absent from sorted CD38-lo luminal cells but evident in organoids derived from CD38-lo luminal cells, related to Figure 2. (A) Single-sorted basal cells and double-sorted CD38-lo luminal cells were plated onto glass slides and cells were stained for the basal antigen p63 (green) and DAPI nuclear counterstain (blue). The percentage of p63+ cells per field is quantified. Statistics represent two-tailed paired t-test, **** represents $p < 0.0001$. (B) Representative images of p63+ basal cells (left) and p63- CD38-lo luminal cells (right) are shown. Scale bars, 50 microns. (C) Representative staining of CD38-lo luminal cell-derived organoids stained for p63 indicates both p63+ and p63- cells. Scale bars, 200 microns.

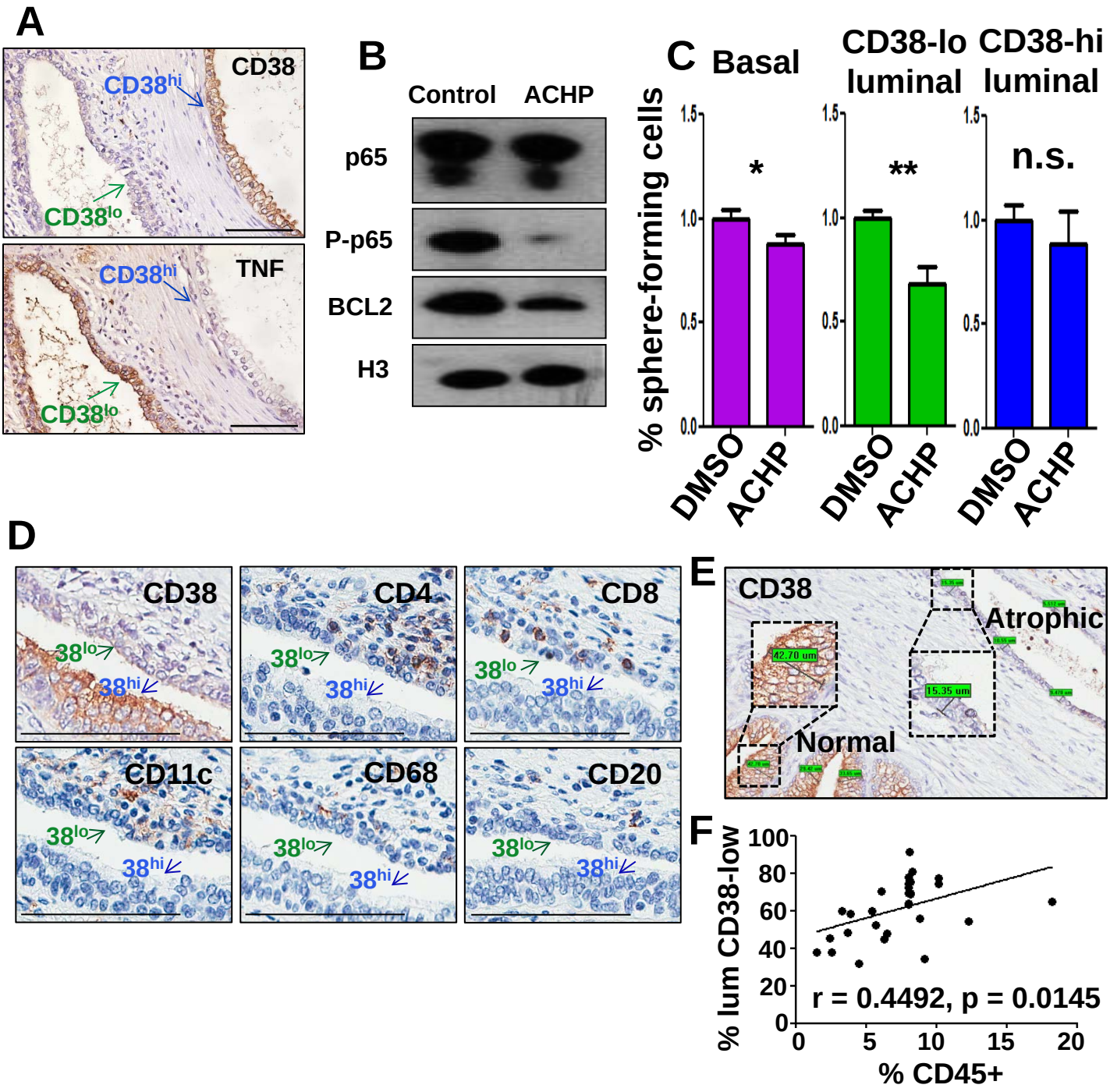

Fig. S3. Inflammatory signaling and inflammation-adjacent location of CD38-lo luminal cells, related to Figure 3. (A) Immunohistochemistry on serial sections of benign human prostate stained for CD38 and TNF alpha indicating mutually exclusive staining patterns. Scale bars, 100 microns. (B) Western blot of CD38-lo luminal cells treated for 4 hours with 5 uM NFkB inhibitor ACHP compared to control. (C) NFkB inhibition reduces organoid-formation of epithelial subsets cells in response to 5 uM ACHP compared to control. Data represent two-tailed unpaired t-test. * p = 0.0441, ** p = 0.0015, n.s. not significant. (D) Immunohistochemistry on serial slides of benign human prostate stained for CD38 and inflammatory cell markers CD4, CD8, CD11c, CD68 and CD20. All scale bars, 100 microns. (E) Immunohistochemical staining for CD38 in normal and atrophic glands with measurements for distances extending from the basement membrane to the lumen shown. (F) Pearson correlation of % CD45+ immune cells and % of luminal cells expressing CD38-lo phenotype in 29 patient samples. r = 0.4492, ** p = 0.0145.

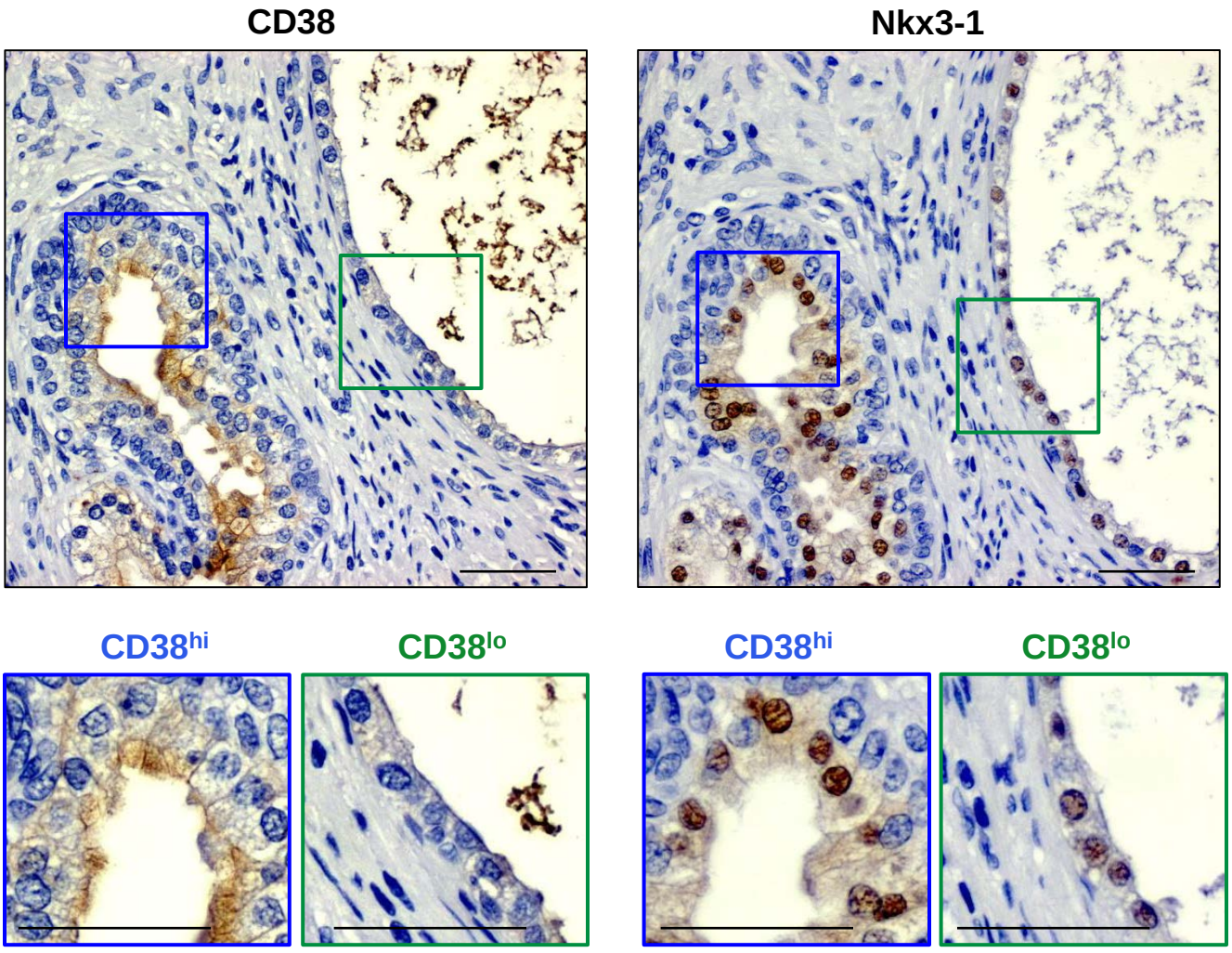

Fig. S4. CD38 and Nkx3-1 expression are correlated in human prostate, related to Figure 4. Serial sections of benign human prostate showing immunohistochemical staining for CD38 and Nkx3-1. Boxed regions are magnified below to demonstrate stronger staining for Nkx3-1 in CD38-hi compared to CD38-lo luminal cells. Scale bars, 50 microns.

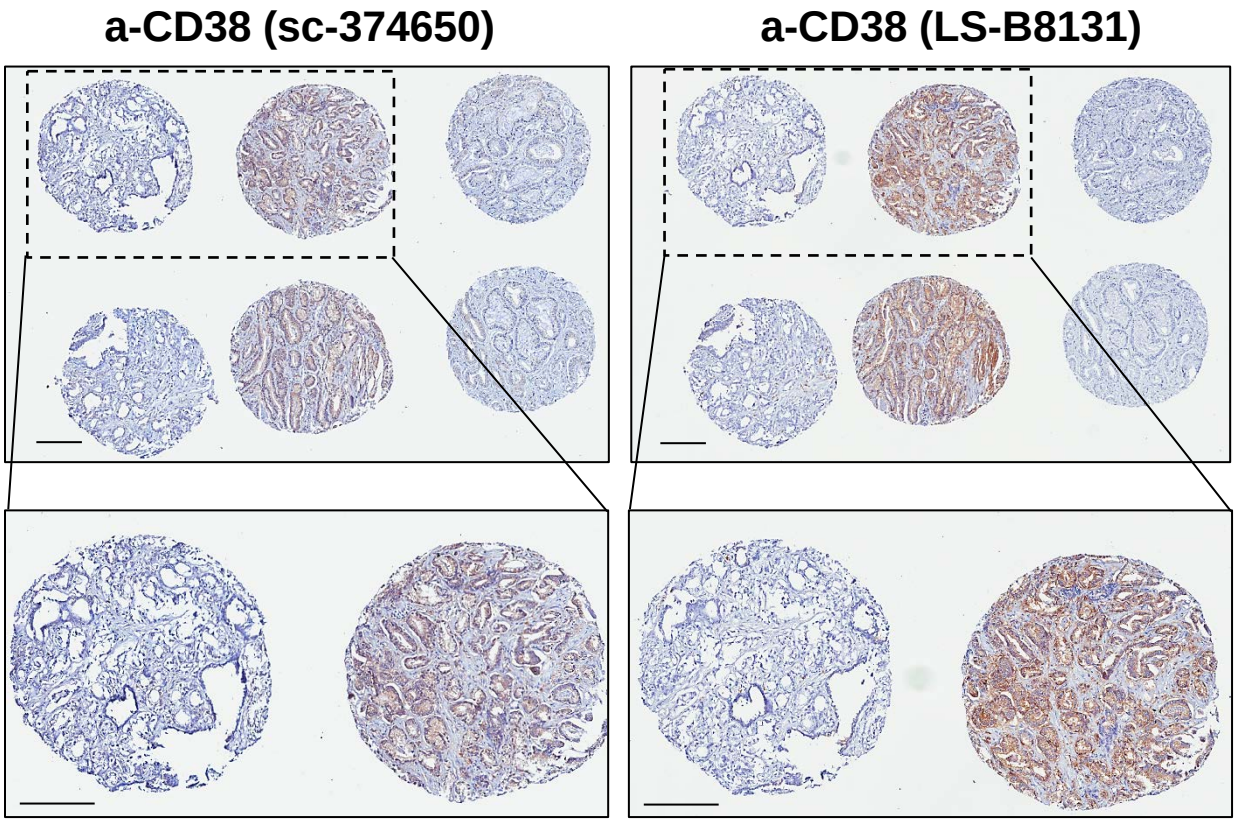

Fig. S5. Two CD38 antibodies give similar results, related to Figure 5. Immunohistochemical staining for CD38 with LifeSpan Biosciences antibody LS-B8131 and Santa Cruz antibody sc-374650 on representative human prostate cancer tissues with higher-power images below. Scale bars, 200 microns.

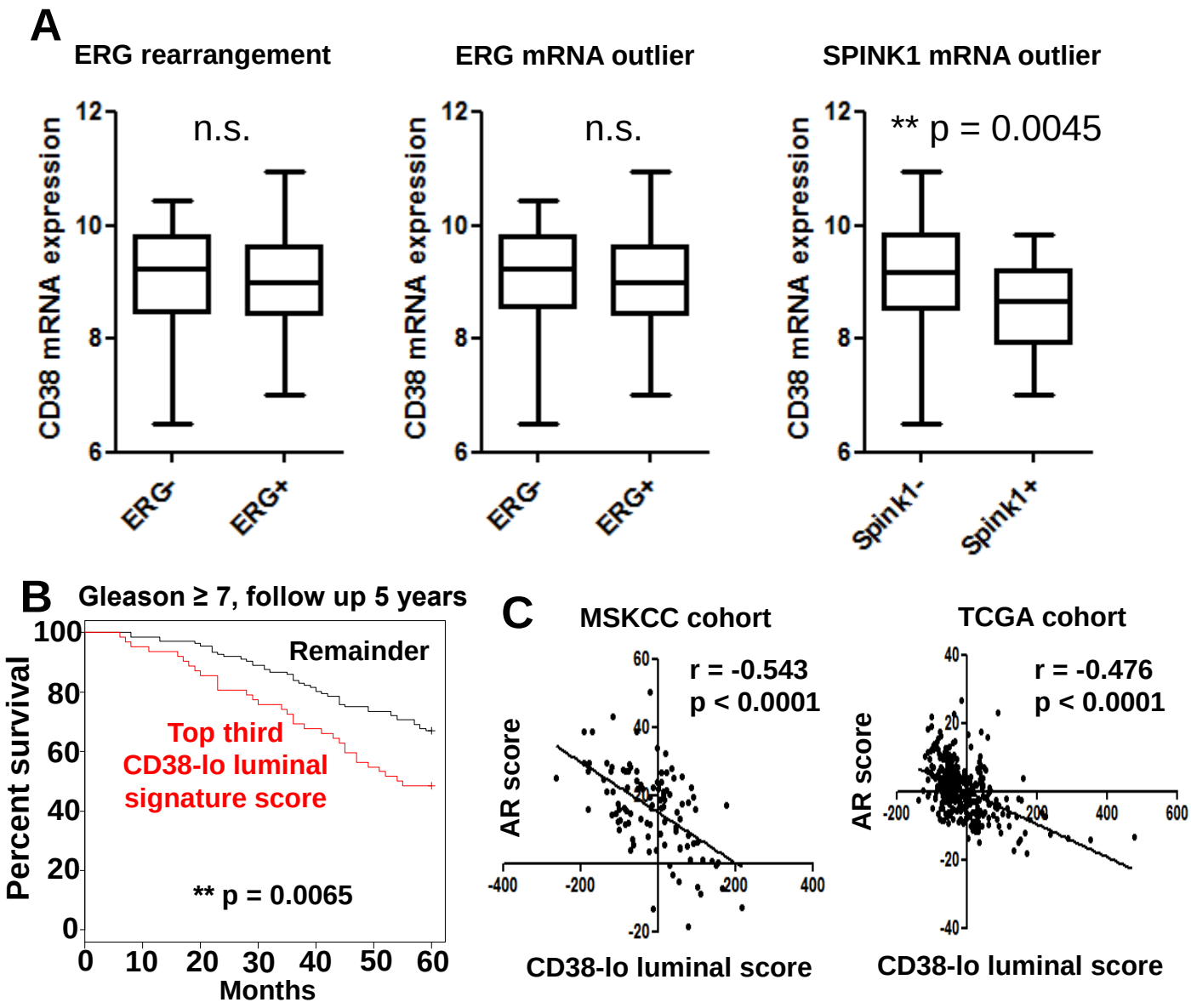

Fig. S6. Correlation of CD38 expression and CD38-lo luminal signature with common alterations, AR signature score and outcome, related to Figure 5. (A) Using cBioportal, primary tumors with mRNA expression in the MSKCC cohort were stratified based on ERG fusion status (left), ERG mRNA outlier status (middle) or SPINK1 outlier status (right). Statistics represent unpaired t test. (B) Survival analysis measuring overall survival of the top third tumors with CD38-lo luminal gene signature (red) compared to the remainder (black) from the Swedish Watchful Waiting cohort, restricted to patients with Gleason greater than or equal to 7 and follow up within 5 years. Log rank p=0.0065. (C) Pearson correlation of CD38-lo luminal signature score with AR signature score in MSKCC and TCGA cohorts.

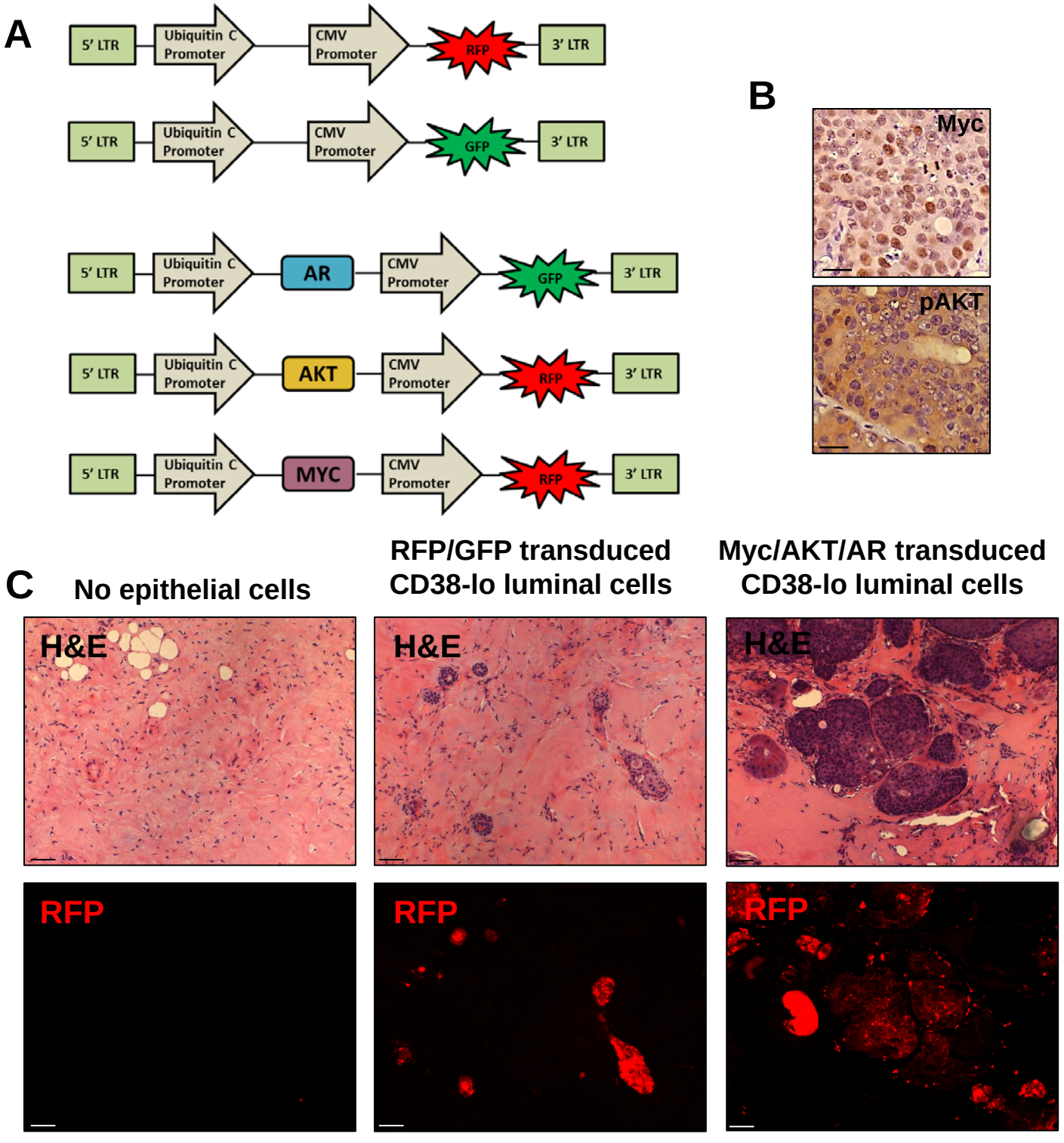

Fig. S7. Fluorescence identifies human epithelial cells in regenerated tissues, related to Figure 7. (A) Schematics of lentiviruses used for in vivo regeneration and transformation related to Figure 3. From top to bottom: FUCRW (RFP), FUCGW (GFP), FU-AR-CGW (AR), FU-AKT-CRW (AKT), FU-Myc-CRW (Myc). (B) CD38-lo luminal cell initiated tumors driven by Myc, AKT and AR stained for oncogenes Myc and AKT. Scale bars, 25 microns. (C) Serial slides stained for H&E or viewed under the fluorescence microscope. In the absence of CD38-lo luminal cells, no epithelial structures are present corresponding to an absence of fluorescence signal. Normal glands in the RFP/GFP group and malignant glands in the Myc/AKT/AR group express varying red fluorescence confirming human epithelial origin. Scale bars, 100 microns.

Supplemental Tables

Table S1. CD38-lo luminal gene signature and RPKM values, related to Figure 3. Table S1A indicates genes listed by official gene symbol or ID and the average fold change for CD38-lo luminal cells compared to CD38+ luminal (middle) or basal cells (right) from three distinct individuals. The signature is restricted to genes with expression in CD38-lo luminal cells that is 2-fold greater than CD38+ luminal and 1.5-fold greater than basal cells. Table S1B (second tab) includes all RPKM values from three patients and fold changes within each patient. See excel file.

Age_GTET65

		Frequency	Percent	Valid Percent	Cumulative Percent
Valid	<65	156	58.4	58.4	58.4
	>=65	111	41.6	41.6	100.0
	Total	267	100.0	100.0	

PSAcat

		Frequency	Percent	Valid Percent	Cumulative Percent
Valid	< 5	56	21.0	21.0	21.0
	5-10	110	41.2	41.2	62.2
	>10	101	37.8	37.8	100.0
	Total	267	100.0	100.0	

GleasonScorecat

		Frequency	Percent	Valid Percent	Cumulative Percent
Valid	<=6	140	52.4	52.4	52.4
	7	113	42.3	42.3	94.8
	>=8	14	5.2	5.2	100.0
	Total	267	100.0	100.0	

ECE on path analysis

		Frequency	Percent	Valid Percent	Cumulative Percent
Valid	No	236	88.4	88.7	88.7
	Yes	30	11.2	11.3	100.0
	Total	266	99.6	100.0	
Missing	System	1	.4		
Total		267	100.0		

Positive surgical margin

		Frequency	Percent	Valid Percent	Cumulative Percent
Valid	No	160	59.9	60.2	60.2
	Yes	106	39.7	39.8	100.0
	Total	266	99.6	100.0	
Missing	System	1	.4		
Total		267	100.0		

SV invasion

		Frequency	Percent	Valid Percent	Cumulative Percent
Valid	No	236	88.4	88.7	88.7
	Yes	30	11.2	11.3	100.0
	Total	266	99.6	100.0	
Missing	System	1	.4		
Total		267	100.0		

CstgCat

		Frequency	Percent	Valid Percent	Cumulative Percent
Valid		8	3.0	3.0	3.0
	T1	112	41.9	41.9	44.9
	T2	146	54.7	54.7	99.6
	T3	1	.4	.4	100.0
	Total	267	100.0	100.0	

Recurrence

		Frequency	Percent	Valid Percent	Cumulative Percent
Valid	No	159	59.6	60.2	60.2
	Yes	105	39.3	39.8	100.0
	Total	264	98.9	100.0	
Missing	System	3	1.1		
Total		267	100.0		

Table S2. Patient characteristics of UCLA Tissue Microarray, related to Figure 5. Table indicates the breakdown of patients based on age, serum levels of prostate-specific antigen (PSA), Gleason score, extracapsular extension on pathological analysis, positive surgical margin, seminal vesicle invasion, Pathologic stage at diagnosis and recurrence status.

Difference		p-value
NL	**Pin**	<0.001
NL	**< 7**	<0.001
NL	**7-10**	<0.001
PIN	**< 7**	0.037
PIN	**7-10**	0.001
7-10	**< 7**	0.070

Table S3. Statistical comparison of CD38 expression between histological grades, related to Figure 5. Statistical analysis comparing the CD38 expression levels between the four different prostate regions (NL, PIN, Gleason < 7, Gleason 7-10) indicates a statistically significant difference between CD38 levels in normal tissue and diseased states.

Univariate model (biochemical recurrence)

CD38 Aggregation	HR (95% CI)	p-value
Mean CA	0.9994 (0.9971, 1.002)	0.595
Overall mean	0.9967 (0.9939, 0.9996)	0.025

Table S4. Association between low protein expression of CD38 and biochemical recurrence, related to Figure 5. Cox proportional-hazards model was used to calculate the association between low expression of CD38 and time to biochemical recurrence. P-values <0.05 were considered statistically significant.

Univariate Cox Regression, **Biochemical Recurrence, MSKCC cohort**

	Sig.	HR	Lower	Upper
low CD38 (z-score less than 1)	0.001	3.665	1.685	7.972

Multivariate Cox Regression with nomogram, **Biochemical Recurrence**

	Sig.	HR	Lower	Upper
low CD38 (z-score less than 1)	0.006	3.023	1.381	6.619
Nomogram score	0.000	0.955	0.942	0.968

Univariate Cox Regression, **Metastasis, MSKCC cohort**

	Sig.	HR	Lower	Upper
low CD38 (z-score less than 1)	0.004	4.729	1.640	13.635

Multivariate Cox Regression with nomogram, **Metastasis**

	Sig.	HR	Lower	Upper
low CD38 (z-score less than 1)	0.030	3.280	1.125	9.559
Nomogram score	0.000	0.960	0.943	0.977

Univariate Cox Regression, **Biochemical Recurrence, MSKCC cohort**

	Sig.	HR	Lower	Upper
CD38 expression (z-score, continuous)	0.001	0.517	0.352	0.759

Multivariate Cox Regression with nomogram, **Biochemical Recurrence**

	Sig.	HR	Lower	Upper
CD38 expression (z-score, continuous)	0.000	0.952	0.939	0.965
Nomogram score	0.000	0.488	0.327	0.728

Univariate Cox Regression, **Metastasis, MSKCC cohort**

	Sig.	HR	Lower	Upper
CD38 expression (z-score, continuous)	0.002	0.394	0.220	0.708

Multivariate Cox Regression with nomogram, **Metastasis**

	Sig.	HR	Lower	Upper
CD38 expression (z-score, continuous)	0.006	0.412	0.218	0.778
Nomogram score	0.000	0.959	0.942	0.977

Univariate Cox Regression, **Biochemical Recurrence, TCGA cohort**

	Sig.	HR	Lower	Upper
CD38 expression (z-score, continuous)	0.015	0.391	0.184	0.832

Table S5. Statistics evaluating CD38 mRNA with patient outcome, related to Figure 5. Table indicates Cox regression analysis for low CD38 (z-score less than 1) or CD38 expression as a continuous variable in the Memorial Sloan-Kettering dataset (Taylor et al, Cancer Cell, 2010; Hieronymus et al, PNAS 2014) and TCGA dataset (TCGA, Cell, 2015). Sig: statistical significance. HR: hazard ratio. Lower/Upper represents 95% confidence interval. Nomogram refers to Stephenson et al prediction for 10-year probability of disease recurrence after prostatectomy including both clinical and pathological variables (Stephenson et al. J Clin Oncol 2005).

A **All patients**

	coef	se (coef)	Z	p-value
Top Third CD38-lo luminal-like	0.3125	0.1498	2.086	0.03699
Gleason Sum	0.5348	0.0693	7.715	1.21E-14
Age	0.0508	0.0111	4.566	4.97E-06
Cancer %	0.0095	0.0031	3.061	0.00221
#HR for tumors in the top third: 1.37 (95% CI: 1.019,1.833)				

B **Gleason >=7, follow up within 5 years**

	coef	se (coef)	Z	p-value
Top Third CD38-lo luminal-like	0.8061	0.2387	3.377	0.0007
Gleason Sum	0.4358	0.1171	3.723	0.0002
Age	0.0492	0.0175	2.815	0.0049
Cancer %	0.0088	0.0043	2.057	0.0397
#HR for tumors in the top third: 2.056 (95% CI: 1.322,3.198)				

C **Gleason >=7, follow up within 5 years (corresponding to Fig S7B)**

	coef	se (coef)	Z	p-value
Top Third CD38-lo luminal-like	0.6203	0.2315	2.68	0.0074
#HR for tumors in the top third: 1.86 (95% CI: 1.181, 2.927)				
Concordance= 0.574 (se = 0.026)				
Rsquare= 0.034 (max possible= 0.981)				
Likelihood ratio test= 6.84 on 1 df, p=0.008928				
Wald test = 7.18 on 1 df, p=0.007371				
Score (logrank) test = 7.41 on 1 df, p=0.006479				

D

All patients					
	coef	se (coef)	Z	p-value	
Top Third CD38-lo luminal-like	0.3355	0.1627	2.0620	0.0392	*
NARP21 immune signature score	0.2915	0.3126	0.9330	0.3510	
AR signature score	-0.0774	0.2734	-0.2830	0.7772	
Gleason Sum	0.5441	0.0702	7.7500	9.21e-15	***
Age	0.0519	0.0112	4.6300	3.65e-06	***
Cancer %	0.0095	0.0031	3.0710	0.0021	**
#HR for tumors in the top third: 1.399 (95% CI: 1.017,1.924)					

E

Gleason >=7, follow up within 5 years					
	coef	se (coef)	Z	p-value	
Top Third CD38-lo luminal-like	0.8389	0.2531	3.3150	0.0009	***
NARP21 immune signature score	0.2766	0.5287	0.5230	0.6009	
AR signature score	0.3452	0.5207	0.6630	0.5074	
Gleason Sum	0.6007	0.1030	5.8340	5.4E-09	***
Age	0.0550	0.0173	3.1890	.00143	**
Cancer %	0.0107	0.0042	2.4930	0.0127	*
#HR for tumors in the top third: 2.314 (95% CI: 1.4089,3.800)					

Table S6. Statistical analysis of CD38-lo luminal gene signature associated with overall survival in Swedish Watchful Waiting cohort, related to Figure 5. (A-B) We performed a multivariate cox model adjusting for Gleason sum, age, and percentage of cancer. (A) When including all patients in the analysis, we found the mean of the scaled expression values of the CD38-lo luminal genes is significantly (p=0.037) associated with all cause mortality. (B) When we restricted analysis to patients with Gleason scores greater than or equal to 7 and a follow-up within 5 years, the mean of the scaled expression values of the CD38-lo luminal genes is significantly (p=0.0007) associated with all cause mortality. (C) Analysis corresponding to Figure S6B comparing the survival of patients in the top third compared to the remainder. (D-E) Multivariate cox model including AR signature score and NARP21 immune signature score related to A-B.